The Plant Cell, Vol. 25: 4305–4323, November 2013, www.plantcell.org

LARGE-SCALE BIOLOGY ARTICLE

Systems-Level Analysis of Nitrogen Starvation–Induced Modifications of Carbon Metabolism in a *Chlamydomonas reinhardtii* Starchless Mutant[W]

Ian K. Blaby,[a] Anne G. Glaesener,[a] Tabea Mettler,[b] Sorel T. Fitz-Gibbon,[a,c] Sean D. Gallaher,[a] Bensheng Liu,[d] Nanette R. Boyle,[a,1] Janette Kropat,[a] Mark Stitt,[b] Shannon Johnson,[e] Christoph Benning,[d] Matteo Pellegrini,[c,f] David Casero,[c,f,2] and Sabeeha S. Merchant[a,f,3]

[a] Department of Chemistry and Biochemistry, University of California, Los Angeles, California 90095
[b] Max Planck Institute for Molecular Plant Physiology, Potsdam-Golm, Germany 14476
[c] Department of Molecular, Cell, and Developmental Biology, University of California, Los Angeles, California 90095
[d] Department of Biochemistry and Molecular Biology, Michigan State University, East Lansing, Michigan 48824
[e] Genome Science, Los Alamos National Laboratory, Los Alamos, New Mexico 87545
[f] Institute of Genomics and Proteomics, University of California, Los Angeles, California 90095

ORCID ID: 0000-0002-2594-509X (S.S.M.).

To understand the molecular basis underlying increased triacylglycerol (TAG) accumulation in *starchless* (*sta*) *Chlamydomonas reinhardtii* mutants, we undertook comparative time-course transcriptomics of strains CC-4348 (*sta6* mutant), CC-4349, a cell wall–deficient (*cw*) strain purported to represent the parental *STA6* strain, and three independent *STA6* strains generated by complementation of *sta6* (CC-4565/*STA6*-C2, CC-4566/*STA6*-C4, and CC-4567/*STA6*-C6) in the context of N deprivation. Despite N starvation–induced dramatic remodeling of the transcriptome, there were relatively few differences (5×10^2) observed between *sta6* and *STA6*, the most dramatic of which were increased abundance of transcripts encoding key regulated or rate-limiting steps in central carbon metabolism, specifically isocitrate lyase, malate synthase, transaldolase, fructose bisphosphatase and phosphoenolpyruvate carboxykinase (encoded by *ICL1*, *MAS1*, *TAL1*, *FBP1*, and *PCK1* respectively), suggestive of increased carbon movement toward hexose-phosphate in *sta6* by upregulation of the glyoxylate pathway and gluconeogenesis. Enzyme assays validated the increase in isocitrate lyase and malate synthase activities. Targeted metabolite analysis indicated increased succinate, malate, and Glc-6-P and decreased Fru-1,6-bisphosphate, illustrating the effect of these changes. Comparisons of independent data sets in multiple strains allowed the delineation of a sequence of events in the global N starvation response in *C. reinhardtii*, starting within minutes with the upregulation of alternative N assimilation routes and carbohydrate synthesis and subsequently a more gradual upregulation of genes encoding enzymes of TAG synthesis. Finally, genome resequencing analysis indicated that (1) the deletion in *sta6* extends into the neighboring gene encoding respiratory burst oxidase, and (2) a commonly used *STA6* strain (CC-4349) as well as the sequenced reference (CC-503) are not congenic with respect to *sta6* (CC-4348), underscoring the importance of using complemented strains for more rigorous assignment of phenotype to genotype.

INTRODUCTION

Starch is the predominant energy storage molecule of photosynthetic organisms in the Viridiplantae, and its synthesis and degradation are well characterized in many organisms, including *Chlamydomonas reinhardtii* (Ball and Deschamps 2009; Zeeman et al., 2010). Starch is formed in the plastid by the sequential activities of ADP-Glc pyrophosphorylase, converting Glc-1-P to ADP-Glc, and starch synthases and starch branching enzymes, which catalyze the formation of α-1,4- and α-1,6-glycosidic bonds, respectively, to generate amylose and amylopectin (Smith, 1999). The genes encoding these enzymes in *C. reinhardtii* have been identified through classical genetics or homology-based approaches. Mutations in either *starchless6* (*sta6*), encoding the small subunit of ADP-Glc pyrophosphorylase, or *sta7*, encoding isoamylase, abolish starch synthesis (Mouille et al., 1996; Zabawinski et al., 2001). The biosynthesis of storage carbohydrate polymers (starch or chrysolaminaran, previously known as leucosin) as well as triacylglycerols (TAGs) is promoted in green algae and diatoms during N starvation as a strategy for storing reduced carbon when there is insufficient N nutrition for growth and division (Varum and Myklestad, 1984; Granum et al., 2002; Guschina and Harwood, 2006; Hu et al., 2008; Rodolfi et al., 2009; Wang et al., 2009; Work et al., 2010; Siaut et al., 2011) .

C. reinhardtii sta mutants and equivalent mutants in other photosynthetic organisms accumulate higher amounts of TAG.

[1] Current address: Chemical and Biological Engineering, Colorado School of Mines, Golden, CO 80401.
[2] Current address: Department of Pathology and Laboratory Medicine, University of California, Los Angeles, CA 90095.
[3] Address correspondence to merchant@chem.ucla.edu.
The author responsible for distribution of materials integral to the findings presented in this article in accordance with the policy described in the Instructions for Authors (www.plantcell.org) is: Sabeeha S. Merchant (merchant@chem.ucla.edu).
[W] Online version contains Web-only data.
www.plantcell.org/cgi/doi/10.1105/tpc.113.117580

It is assumed that this occurs because carbon flow to storage carbohydrate is blocked (Ramazanov and Ramazanov, 2006; Wang et al., 2009; Li et al., 2010a, 2010b; Work et al., 2010; Fan et al., 2011, 2012; Sanjaya et al., 2011). The increased yield of TAG in acetate-supplemented N-starved *sta6* is not inconsistent with this model (Goodson et al., 2011; Ramanan et al., 2013). Because of the potential for using algae to generate biodiesel precursors, there is interest in understanding carbon metabolism and its regulation in the context of TAG accumulation in algae (reviewed in Johnson and Alric, 2013). In addition to triggering starch and TAG synthesis, N starvation also induces a number of other responses, including ribosome turnover, gametogenesis, and chlorosis (Siersma and Chiang, 1971; Martin and Goodenough, 1975; Plumley and Schmidt, 1989; Bulté and Wollman, 1992).

C. reinhardtii, a unicellular chlorophyte alga containing a pyrenoid within its single chloroplast representing the site of starch accumulation and ribulose-1,5-bis-phosphate carboxylase/oxygenase function, is an excellent reference system for addressing this issue (Harris, 2001). A draft genome sequence (http://www.phytozome.net/search.php for the version 5 assembly), resources for transcriptomics, proteomics, metabolomics (Bölling and Fiehn, 2005; May et al., 2008; Atteia et al., 2009; Rolland et al., 2009; Mühlhaus et al., 2011; Urzica et al., 2012; Wang et al., 2012), and well-characterized mutants in starch metabolism are available (Ball et al., 1991; Mouille et al., 1996; Wattebled et al., 2002, 2003). In addition, the growth medium and nutrient requirements are well defined, and there is considerable ongoing effort to discover and understand the operation of carbon metabolism pathways under different trophic situations, including anaerobiosis, respiratory, and phototrophic conditions (Kropat et al., 2011; Brueggeman et al., 2012; Catalanotti et al., 2012; Fang et al., 2012; Johnson and Alric, 2012). Recent investigations of TAG accumulation have documented two sites for lipid droplet accumulation in *C. reinhardtii*, one extraplastidic, likely in endoplasmic reticulum–derived compartments, and the other within the chloroplast (Li-Beisson et al., 2010; Fan et al., 2011; Goodson et al., 2011). The plastid lipid bodies are more evident in *sta6*, again consistent with the redirection of reduced carbon from starch (synthesized in the plastid) to TAG accumulation (Goodson et al., 2011).

Although N starvation is the best trigger for TAG accumulation in *C. reinhardtii* under both photoautotrophic or photoheterotrophic growth conditions, other nutrient deficiencies also promote TAG biosynthesis, including P, S, Fe, and Zn starvation (Matthew et al., 2009; Kropat et al., 2011; Breuer et al., 2012; Cakmak et al., 2012; Msanne et al., 2012). Recent transcriptome experiments have sought to identify the key acyltransferases and other proteins involved in algal TAG accumulation and lipid body biosynthesis (Miller et al., 2010; Boyle et al., 2012). These studies have resulted in the identification of both type I and type II acyltransferases, DGAT1 and DGTT1 through DGTT5, respectively, for de novo TAG biosynthesis, where TAG is synthesized from diacylglycerol and acyl-coenzyme A (acyl-CoA), as well as a phospholipid diacylglyceroltransferase, PDAT1, in which TAG is synthesized by transesterification using a membrane lipid as a substrate (Miller et al., 2010; Merchant et al., 2012; Boyle et al., 2012; Msanne et al., 2012; Yoon et al., 2012).

With a view to understanding the effect of redirecting carbon from starch biosynthesis toward TAG accumulation, we used comparative transcriptomics of the *sta6* mutant and its presumed parental strain in a time course of N starvation to distinguish *sta6*-dependent differences. We validated the discoveries by documentation of changes in enzyme activity and selected metabolites to conclude that gluconeogenesis is counterintuitively stimulated in the *sta6* mutant. In the course of the work, we also discovered that strain CC-4349, originally listed in the culture collection as the parent of *sta6*, is mislabeled. Genome resequencing identified strain CC-4568 as the true parent. Therefore, we compared the *sta6* mutant to three independent complemented strains to understand the contribution of the *STA6* locus to the phenotype. Genome resequencing and transcriptomics give an indication of the variability between individual transformants, which may be useful in other work.

RESULTS

Comparative Transcriptomics of CC-4349, *sta6*, and Three Independent STA6 Strains under N Deprivation

The *sta6* mutant, which is incapable of starch synthesis because of a mutation in the small subunit of ADP-Glc pyrophosphorylase, can accumulate only TAG when it is starved for N (Zabawinski et al., 2001). Several studies indicate that this and other *sta* mutants accumulate more TAG than do the corresponding wild-type or complemented strains (Wang et al., 2009; Li et al., 2010b; Work et al., 2010). When we transferred the *sta6* mutant (CC-4348), a wild-type presumed parental strain (but see below), CC-4349, and three previously characterized complemented strains *STA6*-C2, *STA6*-C4, and *STA6*-C6 (CC-4565, CC-4566, and CC-4567, respectively) to Tris-acetate-phosphate (TAP) medium lacking ammonium (the usual N source), we recapitulated this phenotype (Figure 1). None of the strains grows appreciably in N-free medium, experiencing at most one doubling during the course of the experiment (48 h). Chlorophyll content decreased in all strains, and consistent with a previous report, the decrease of chlorophyll is slightly accelerated in the *sta6* mutant (Work et al., 2010). As expected, the starch content increased rapidly in *STA6* strains as a function of time after transfer to N-free medium but was near zero in the *sta6* mutant strain (Zabawinski et al., 2001). Although we did not measure a significant difference in TAG accumulation in CC-4349 versus *sta6* in the first 48 h after N deprivation, we noted that by 96 h, the TAG content of *sta6* exceeded that of CC-4349 (52 versus 24 fmol cell^{-1}, respectively) (Figure 1D), as documented by others (Li et al., 2010a; Work et al., 2010). *sta6* accumulated more major lipid droplet protein (MLDP1), a protein associated with the algal lipid droplet, than did *STA6* (Figure 1E).

In previous work, we identified several genes, *DGAT1*, *DGTT1*, and *PDAT1*, encoding acyltransferases whose expression was increased in *C. reinhardtii* in response to N removal from the medium, and in a time course experiment established that changes in transcript abundance preceded changes in TAG accumulation (Boyle et al., 2012). Based on that work, we

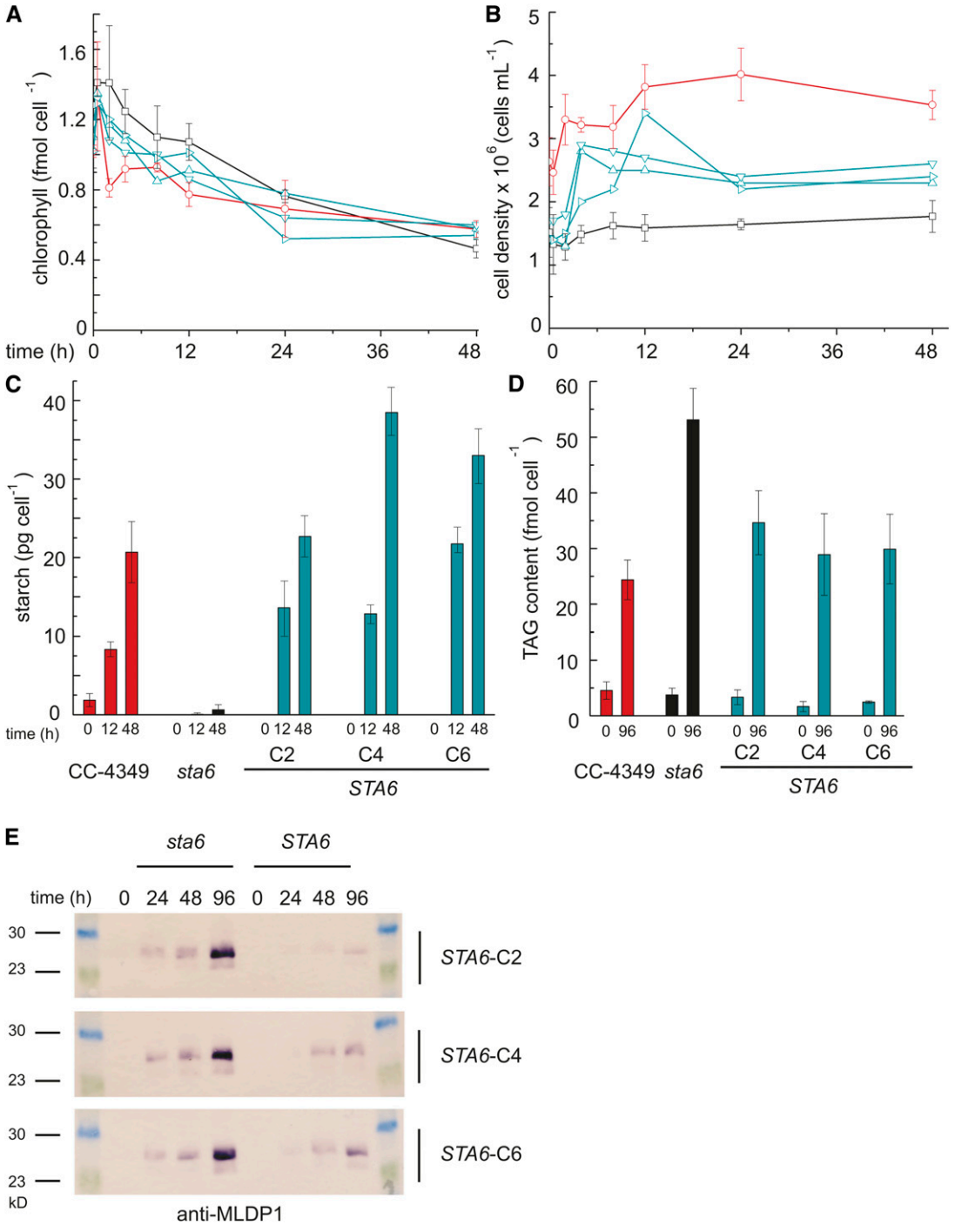

Figure 1. Increased TAG but Not Starch in the *sta6* Mutant.

In all panels, CC-4349 is shown in red, *sta6* (CC-4348) in black, and three strains complemented for *STA6* (*STA6*-C2, *STA6*-C4, and *STA6*-C6) in blue. Chlorophyll content **(A)**, cell density **(B)**, starch content per cell **(C)**, and TAG per cell **(D)**. Error bars represent one SD calculated from three separate cultures (biological replicates). **(E)** shows an immunoblot of MLDP1 using protein extracts obtained from N-deprived cultures of *sta6* and *STA6*-C2, *STA6*-C4, and *STA6*-C6, sampled at 0, 24, 48, and 96 h as indicated.

analyzed the transcriptomes of *sta6*, strain CC-4349, and the three complemented strains in response to N deprivation in a time-course experiment that would allow us to distinguish primary responses as well as longer term ones (Figure 2). Therefore, we collected cells from triplicate cultures of *sta6* and CC-4349 prior to washing in N-free medium (0') and at 0, 0.5, 4, 8, 12, 24, and 48 h after transfer to N-free medium for preparation of total RNA. Additionally, in a second time-course experiment, cells were collected from cultures of *sta6*, CC-4349, *STA6*-C2, *STA6*-C4, and *STA6*-C6 at 0.5, 4, and 48 h after transfer to N-free medium. For strains *sta6* and CC-4349 in the first time-course experiment, two of the RNA preparations were analyzed by RNA sequencing (RNA-Seq) on the Illumina platform, and the third sample was retained for independent validation by quantitative RT-PCR (qRT-PCR), while single samples were taken for cultures of *sta6* and the *STA6* strains collected at 0.5, 4, and 48 h. The reads (totaling 146,992,656 and 447,140,526 for *sta6* and CC4349 in the first experiment and 87,214,220, 91,346,488, 123,682,836, and 131,687,452 for *sta6*, *STA6*-C2, *STA6*-C4, and *STA6*-C6, respectively, in the second experiment; see Supplemental Data Set 1 online) were aligned to the genome and to the 17,301 gene models in the version 4 assembly of the *C. reinhardtii* genome, normalized, and quantified for gene expression estimates (see Methods).

N-Deprivation Responses Unique to CC-4349 and *sta6*

A key objective of this investigation was to identify the effect of the mutation in *STA6* on the N-deficiency transcriptome. Therefore, we used a hierarchical clustering method to retrieve all genes that were expressed differently in the two strains (see Supplemental Figure 1 online).

The analysis revealed a small number of genes encoding enzymes in central carbon metabolism as being differently expressed in *sta6* versus CC-4349 and *STA6*. *ACS3* and *PAT2*, encoding acetyl-CoA synthetase and phosphate acetyl-transferase, which catalyze acetate assimilation, are upregulated severalfold at 24 h in *sta6* compared with CC-4349, reaching 543 versus 149 reads per kilobase of mappable length per million aligned reads (RPKM) and 61 versus 37 RPKM, respectively, and approximately twofold higher at 48 h in *sta6* versus *STA6* (Figure 3; see Supplemental Figure 2 online). Transcripts encoding two enzymes of the glyoxylate cycle, which enables the conversion of the activated acetyl group to gluconeogenic precursors, are more abundant in *sta6* compared with CC-4349. *ICL1* and *MAS1*, encoding isocitrate lyase and malate synthase (both of which are unique to the glyoxylate pathway), are upregulated 12- and 14-fold, respectively, at 48 h, relative to CC-4349, peaking at 700 and 224 RPKM. *PCK1* and *FBP1*, encoding phospho*enol*-pyruvate carboxykinase and Fru-1,6-bisphosphatase, respectively, catalyzing two steps unique to gluconeogenesis, and *TAL1*, encoding transaldolase, cocluster with *ICL1* and *MAS1* with respect to expression pattern and are also ~10-fold upregulated in *sta6* compared with CC-4349 (Figure 3; see Supplemental Data Set 2 online). The transcript abundances of each of these genes are severalfold higher in *sta6* than in *STA6* at 48 h (Figure 3; see Supplemental Figure 2 and Supplemental Data Set 3 online). Four of the five enzymes encoded by these upregulated transcripts are predicted to localize to the chloroplast (see Supplemental Data Set 3 online). All five genes display strikingly similar patterns of expression, consistent with a pathway connection, and suggesting the potential for increased movement of carbon in the direction of gluconeogenesis (Figures 3 and 4). Additionally, *PGH1*, encoding enolase, is upregulated approximately twofold in *sta6* versus CC-4349 (peaking at 1168 and 543 RPKM in the two strains, respectively, at 4 h). With respect to other transcripts encoding enzymes of glycolysis/gluconeogenesis and the pentose phosphate pathway, all are found at similar levels in both strains (see Supplemental Data Set 3 online).

The coordinated increase in transcripts encoding these enzymes in *sta6* versus *STA6* suggests an increase in acetate utilization in the glyoxylate cycle followed by gluconeogenesis to generate hexose-phosphates in *sta6* (Figures 3 and 4). This is counterintuitive given that *sta6* is unable to utilize hexose-phosphate for starch synthesis. These results contrast with the findings from previous studies on *STA6* lines in which transcripts encoding enzymes of the glyoxylate cycle were decreased in -N compared with +N (Miller et al., 2010), indicating that the phenomenon is *sta6* specific.

There is no difference in the abundance of transcripts encoding enzymes of the citric acid cycle, suggesting that acetate oxidation is similar in *sta6* and CC-4349 (see Supplemental Data Set 3 online). Transcripts encoding enzymes of the Calvin Benson cycle are typically decreased in abundance across the time course in both strains, consistent with the rapid downregulation of the genes encoding components of the light reactions (see Supplemental Data Set 4 online).

Surprisingly, the abundance of transcripts encoding enzymes in fatty acid and lipid metabolism were similar in *sta6* versus CC-4349

Figure 2. Experimental Design for Sampling the Transcriptome.

Cultures were grown to a density of 4×10^6 cells mL^{-1} in +N medium and washed in N-free medium before resuspending cells to a final density of 2×10^6 cells mL^{-1} in N-free medium. For the time-course experiment comparing CC-4349 and *sta6*, samples were taken in triplicate at 0' (i.e., from +N medium before washing), 0, 0.5, 2, 4, 8, 12, 24, and 48 h after N deprivation as indicated with red arrows. In a separate experiment, *sta6*, *STA6*-C2, *STA6*-C4, and *STA6*-C6 were sampled at 0.5, 4, and 48 h after N deprivation, as indicated with blue arrows. The light-green color of an N-free culture at 48 h indicates the cells are chlorotic.

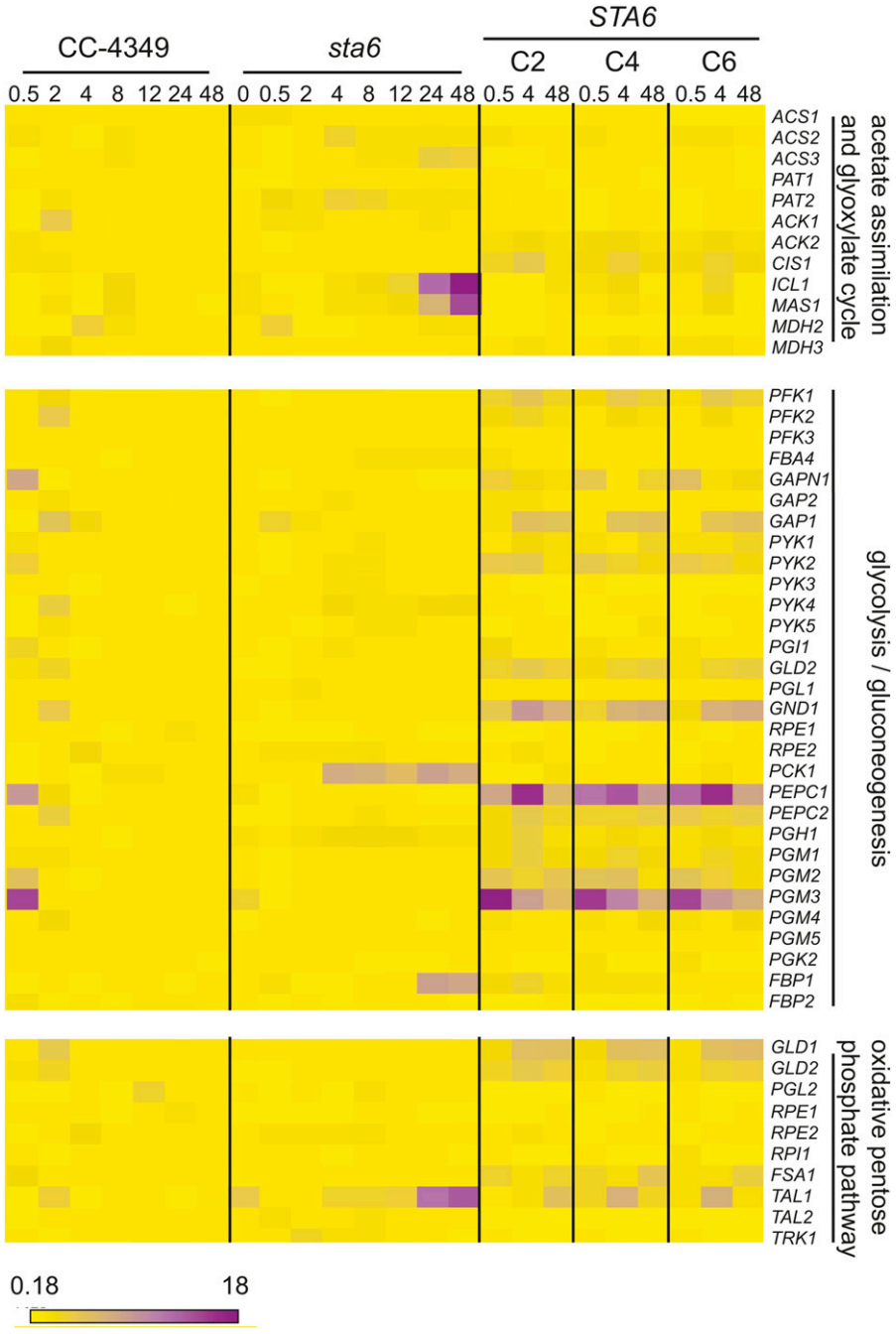

Figure 3. Greater Upregulation of Genes Encoding Enzymes of Acetate Metabolism, Gluconeogenesis, and the Oxidative Pentose Phosphate Pathway in *sta6* versus CC-4349 and *STA6*.

Heat map showing fold change of RPKM (relative to 0 h in CC-4349), ranging from 0.18 (yellow) to 18 (violet), of genes involved in acetate assimilation, the glyoxylate cycle, glycolysis/gluconeogenesis, and the oxidative pentose phosphate pathway as indicated. Heat map was generated using Matrix2png (Pavlidis and Noble, 2003). RPKM values for complete pathways are shown in Supplemental Data Set 3 and Supplemental Figure 2 online.

despite the TAG overaccumulation phenotype of *sta6* (see Supplemental Data Set 5 online). The expression profiles of the four acetyl-CoA carboxylase subunits, and most diacylglycerol acyltransferases (DAGATs) responsible for the final step of TAG synthesis, are highly comparable. Three exceptions to this were *DGTT2*, *Cre06.g310200*, and *MLDP1* for which the transcript numbers are higher in *sta6* versus CC-4349 and *STA6* (Figure 5; see Supplemental Data Set 5 online). *DGTT2* was originally predicted to encode a type-2 diacylglycerol transferase (DGAT) on the basis of high sequence similarity to a protein exhibiting

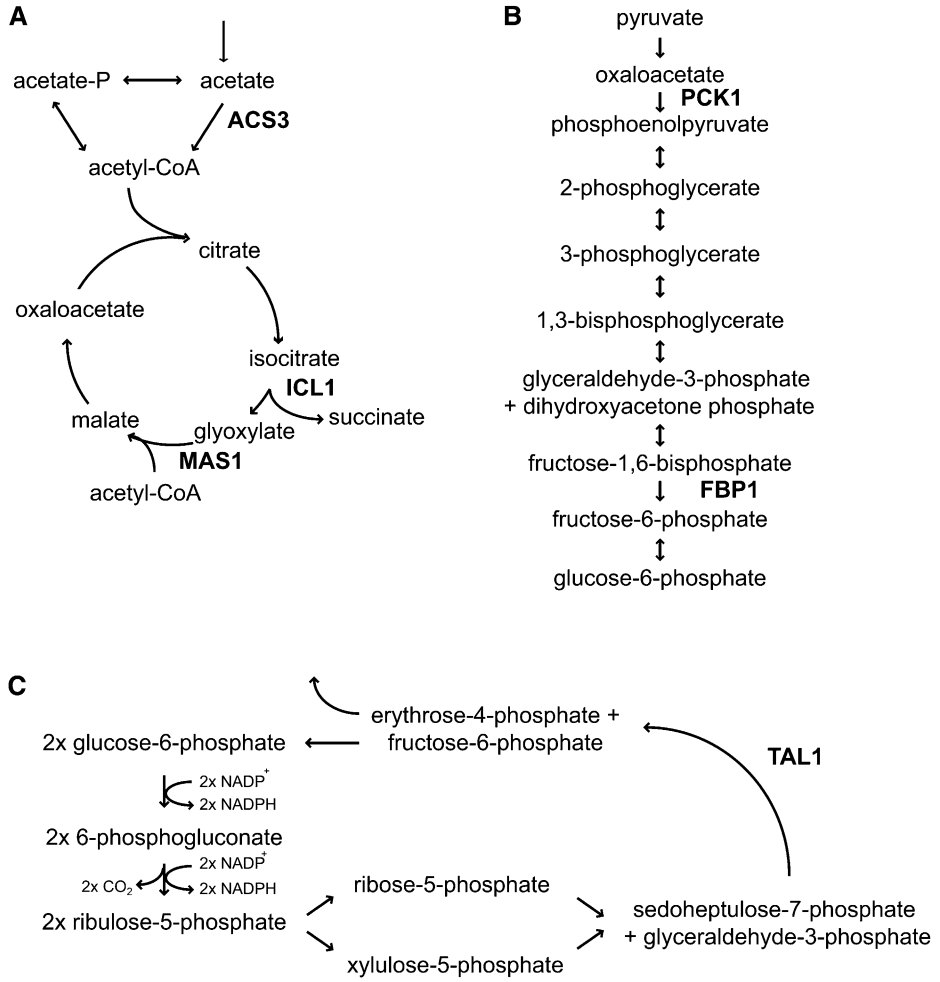

Figure 4. Upregulated Genes Encode Key Enzymes in Central Carbon Metabolism.

Steps in the glyoxylate cycle **(A)**, gluconeogenesis **(B)**, and oxidative pentose phosphate pathway **(C)** are shown. The complete oxidative pentose phosphate pathway is shown in Supplemental Figure 11 online. For clarity, only relevant enzymes are shown.

acyltransferase activity in *Morterialla ramanniana* and has since been functionally validated (Lardizabal et al., 2001; Sanjaya et al., 2013) *Cre06.g310200* possesses high similarity to a type-3 DGAT. Acyltransferase activity has been demonstrated for type-3 DGATs in several organisms, although not yet in an alga (Saha et al., 2006; Rani et al., 2010; Hernández et al., 2012). MLDP1 has been suggested to play a structural role in the algal lipid body analogous to that of oleosins in land plants (Moellering and Benning, 2010). Immunoblot analysis validated that the increased *MLDP1* mRNA abundance is correlated with increased polypeptide accumulation in *sta6* versus *STA6* (Figure 1E), which is consistent with its proposed function as a structural protein of the lipid body. Additionally, the mRNA predicted to encode biotin synthase (Cre01.g261150) accumulates to a threefold higher level in *sta6* than in CC-4349 at several time points. As acetyl-CoA carboxylase is biotin dependent, this suggests the possibility that the cofactor could be rate-limiting.

In response to N starvation, vegetative *C. reinhardtii* cells differentiate into gametes whose mating type is determined by one of two mating loci (called plus and minus) (Sager and Granick, 1954; Beck and Haring, 1996). Gametes subsequently fuse to form zygotes (reviewed in Pan and Snell, 2000). We noted that *SAD1*, *GSM1*, and *FUSM*, all specific to the minus mating type, are expressed in CC-4349 (Ferris and Goodenough, 1994; Ferris et al., 1996; Lin and Goodenough, 2007). Curiously, these genes were not expressed in either *sta6* or in strains complemented for *STA6*. Instead, *MTA3A*, located within the mt^+ locus (Ferris et al., 2002), is expressed in *sta6* and the complemented strains but not in CC-4349 (see Supplemental Data Set 6 online). Indeed, qRT-PCR analysis confirmed that CC-4349 is mt^-, while *sta6* and the *STA6* strains are mt^+ (see Supplemental Figure 3 online).

Genome Sequences Reveal Mutations besides *STA6* Deletion

In addition to the mating type discrepancy, we noted that *sta6* cells are smaller than CC-4349. A small cell size was observed

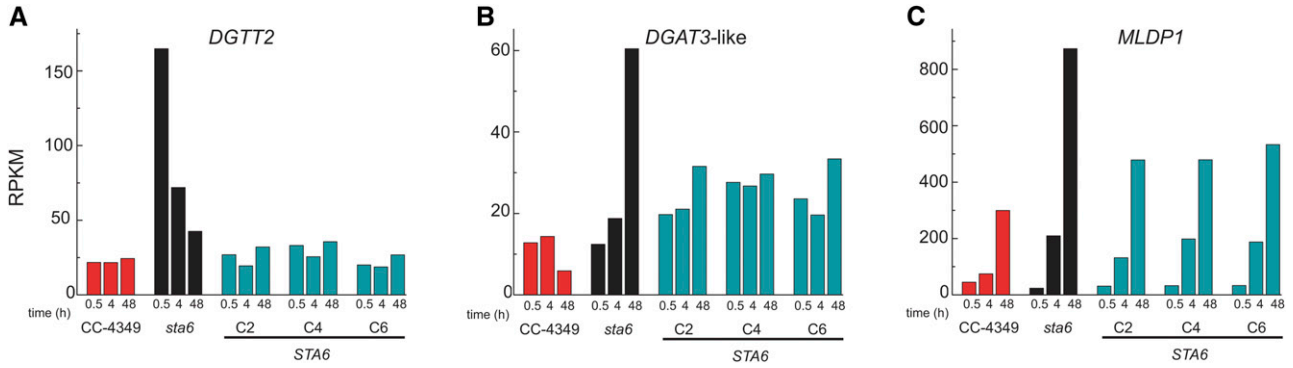

Figure 5. Expression Profiles of Genes Related to TAG Accumulation.

DGTT2, encoding a type-2 diacylglycerolacyltransferase **(A)**; *DGAT3*, encoding a putative soluble diacylglycerolacyltransferase **(B)**; and *MLDP1* encoding major lipid droplet protein **(C)**. Expression level is expressed as RPKM for each mRNA at 0.5, 4, and 48 h. CC-4349 is in red, *sta6* is in black, and *STA6* is in blue.

already by others for *sta6* and *sta7* (another starchless mutant), although CC-124 rather than the parental was used as a wild-type comparison (Work et al., 2010). The small cell size phenotype was not rescued by the *STA6* gene (see Supplemental Figure 4 online). CC-4349 is also not an Arg auxotroph, as described in the original publication, although this was assumed to be the result of a reversion in the laboratory (U. Goodenough, personal communication). Therefore, we resequenced the genomes of *sta6*, the purported wild-type (CC-4349) strain and one of the three complemented *STA6* strains (*STA6*-C6; CC-4567). The original parental *cw* strain from which *sta6* is derived was acquired independently from the Dauvillée laboratory (CC-4568) and was also resequenced (see Methods and Supplemental Table 1 online).

The *sta6* strain was generated by insertion of pARG7.8 into the genome of CC-4568 (Zabawinski et al., 2001). The read coverage validates the insertion of this plasmid in the *sta6* genome and furthermore identified the position of integration, which is in the fourth exon of *STA6* (Figure 6; see Supplemental Table 2 online). The read coverage dropped from >50× in the flanking upstream region to 0 at this locus (genome v5.3 coordinates: chromosome 3, 5742415 to 5748751). However, the drop in coverage extended beyond the *STA6* gene into the neighboring *RBO1* gene. Reads could be aligned throughout this region in all other strains, indicating the reduction in read alignment was not due to difficulty in sequencing the area or attributable to problematic alignment to the reference genome (CC-503). The loss of these two genes from the genome of *sta6* is supported by very low abundance of the corresponding transcripts in the *sta6* transcriptome (see Supplemental Figure 5 online). In addition, transcript abundance of the paralogous *RBO2* gene downstream of *RBO1* was also reduced (peaking at 19 RPKM in CC-4349 but only 1 RPKM in *sta6*), perhaps revealing regulation of *RBO2* by *RBO1*. Besides this issue, we noted a large number of insertions and deletions (InDels) and single-nucleotide variations between *sta6* and the reference strain as well as between *sta6* and CC-4349, the purported parental wild-type strain used also in other studies of TAG accumulation (Wang et al., 2009; Goodson et al., 2011) (see Supplemental Table 2 online). The genome of CC-4568 revealed 15,095 single-nucleotide variants (SNVs) relative to the reference genome (Table 1). This compared with 14510, 15,049, and 15,878 SNVs for *sta6*, *STA6*-C6, and CC-4349, respectively, versus the reference. A pairwise analysis of all genomes indicated 1408 SNVs between CC-4568 and *sta6*, and 2086 between *STA6*-C6 and CC-4568, strongly suggesting that CC-4568 is more closely related to *sta6* and that CC-4349 is more distantly so (Table 1; see Supplemental Figure 6 online).

Analysis of the *STA6*-Complemented Strains

Because genome resequencing analysis indicated a large number of SNVs as well as InDels between CC-4349 and *sta6*, consistent with the conclusion that CC-4349 is not the parental source of the *sta6* mutant, we wondered whether differences in the transcript profiles could truly be attributed to the loss of function in *sta6*. Therefore, we focused our analysis on the transcriptomes of N-free *sta6* and the three *STA6*-complemented strains, *STA6*-C2, *STA6*-C4, and *STA6*-C6. After normalizing the raw data, we generated lists of differentially expressed genes and identified 521 that were common to all three *STA6* strains, representing the true set of differentially expressed genes. Thus, only a small fraction of genes that are differentially expressed between CC-4349 and *sta6* are attributable to the mutation at the *STA6* locus (Figure 7; see Supplemental Data Set 7 online). In addition to the *STA6* locus itself, this intersect includes many of the genes that were differentially expressed between CC-4349 and *sta6* as discussed above, and especially *MAS1*, *ICL1*, *TAL1*, *FBP1*, and *PCK1*.

To summarize this data set, ontology-assigned annotations of restored expression resulting from *STA6* complementation indicate that the loss of the wild-type gene is responsible for the differential expression of genes relating to a number of functional groupings, including lipid metabolism and pathways of central carbon metabolism as noted above (Figure 7B).

To test the effect of the coordinate and striking increase in the expression of *ICL1* and *MAS1* in *sta6* versus *STA6*, we measured the activities of the corresponding enzymes in protein

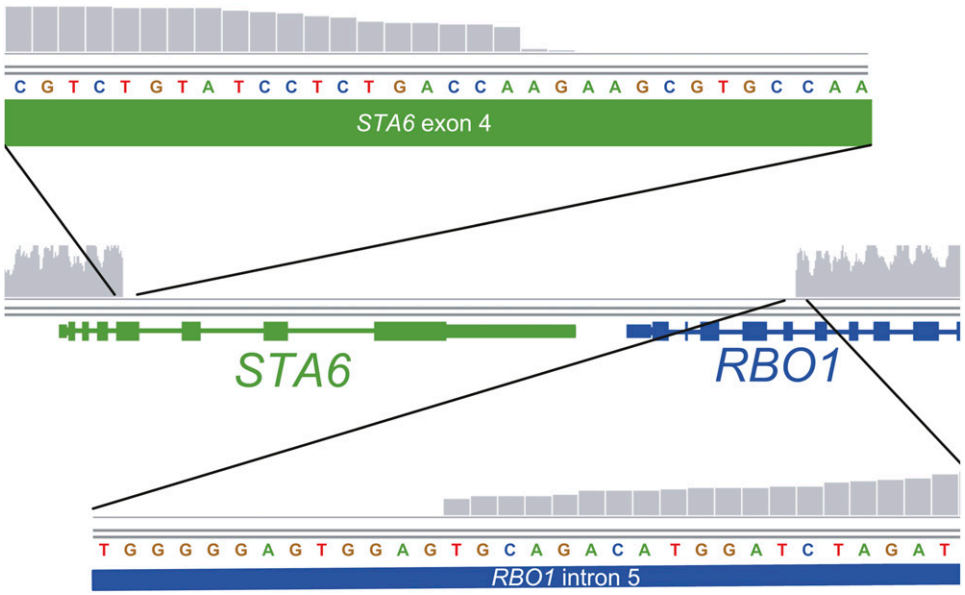

Figure 6. Resequencing of the *sta6* Genome Reveals Extent of Gene Disruption.

The reads were aligned to the *C. reinhardtii* reference strain (CC-503) using the Burrows-Wheeler Aligner and displayed via the Integrative Genomics Viewer. The depth of coverage, indicated in the figure by vertical gray bars on a scale from 0 to 100, drops off precipitously at the boundaries of the disrupted genes. The breakout tracks above and below display the left and right boundaries, respectively, magnified to the nucleotide level. Gene models for *STA6* and *RBO1* are shown with exons represented by thick bars and introns represented by thin bars. The nucleotide track indicates the reference sequence at these loci.

extracts from N-free *sta6* and the three *STA6* strains. We reasoned that as the increased abundance of *ICL1* and *MAS1* transcripts in *sta6* versus CC-4349 is evident ~24 and 48 h after N deprivation, and since changes in transcript abundance should precede changes in protein abundance, we should test protein activities in samples at time points beyond those used for the transcriptome experiments (Figure 8). At 0 h, activity of the two enzymes remained similar in each strain. However, activity of isocitrate lyase increased approximately twofold in *sta6* compared with *STA6* at 48 h and approximately fourfold for malate synthase (Figure 8). A previous comparative proteomic investigation of *cw15* and *sta6* by another group did not identify significant increases in either of these proteins compared with *cw15*, although the cultures were not N starved in that work (Wang et al., 2012). These data confirm that the increase in transcript abundance translates to an increase in enzyme activity, which would suggest that in *sta6*, there might be increased acetate movement toward gluconeogenic precursors via the glyoxylate cycle. We note that transcripts encoding two of the regulated and unique enzymes in the gluconeogenic direction, *FBP1* and *PCK1*, also increased in coordination with *ICL1* and *MAS1* (see Supplemental Data Set 3 and Supplemental Figure 2 online).

Metabolite Analysis Validates the Effect of Transcriptome Changes on Carbon Movement

The effect of the above-mentioned transcriptome changes was validated by liquid chromatography–tandem mass spectrometry (LC-MS/MS) analysis of specific metabolites in *sta6* versus *STA6* grown for 48 h in N-replete and N-free media. First, *sta6* indeed contains far less ADP-Glc (3.0 μM in *sta6* versus 32.6 μM in *STA6* in N-free conditions) as expected from a mutation in ADP-Glc pyrophosphorylase (Figure 9). The residual ADP-Glc might be derived from a low activity of other genes encoding ADP-Glc pyrophosphorylase activities or from side reactions of UDP-Glc pyrophosphorylase in the cytosol. Second, malate and succinate, which are products of the glyoxylate pathway, also increased in *sta6* compared with *STA6*, consistent with increased

Table 1. Pairwise Analysis of SNVs in Each Strain Relative to CC-503

Strain	CC-503[a]	CC-4567 (*sta6*-C6)	CC-4568	CC-4349
CC-503[a]				
CC-4567 (*sta6*-C6)	15,049			
CC-4568	15,095	2,086		
CC-4349	15,878	21,759	21,750	
CC-4348 (*sta6*)	14,510	1,434	1,408	21,145

[a]CC-503 is the sequenced reference strain (Merchant et al., 2007).

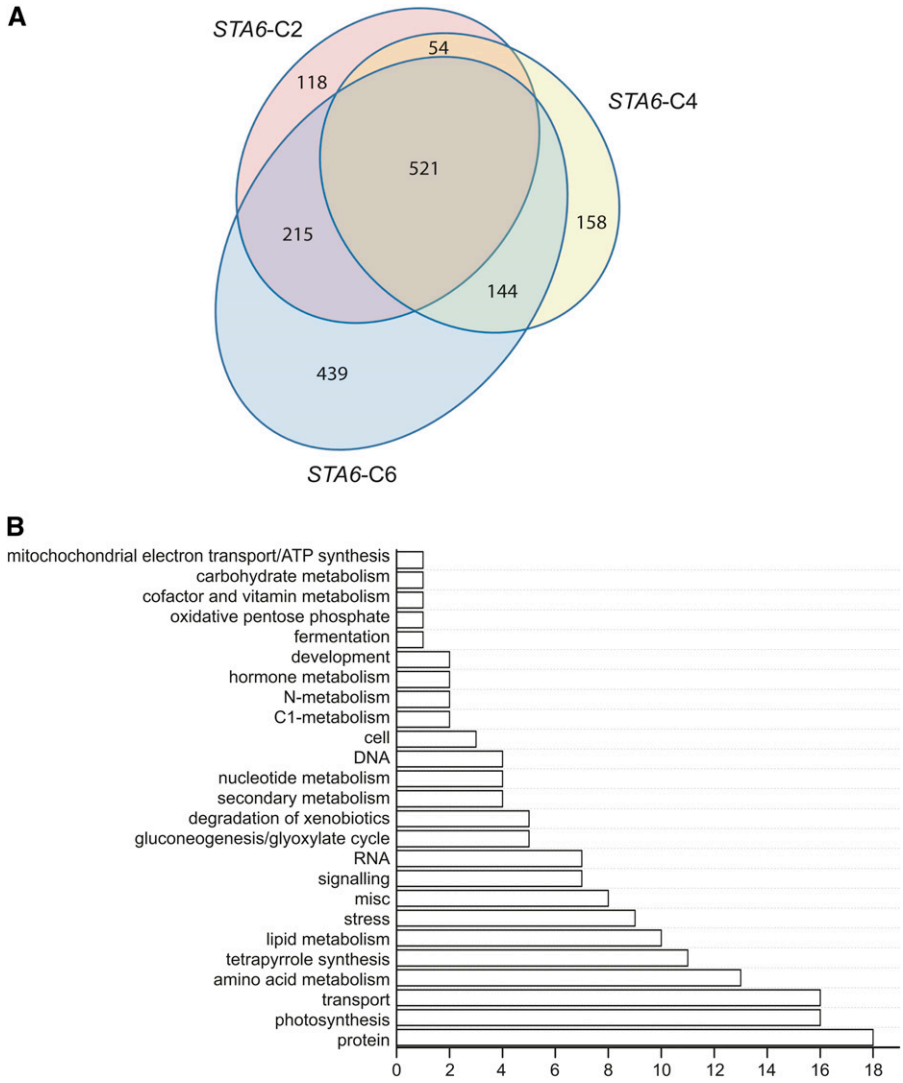

Figure 7. Comparative Analysis of *sta6* and *STA6* Transcriptomes Identifies *sta6*-Dependent Expression Patterns.

(A) Venn diagram showing genes differentially expressed between *sta6* and *STA6*-C2, *STA6*-C4, and *STA6*-C6 at 0.5, 4, and 48 h after N deprivation. The central intersect indicates the differentially expressed genes common to all *STA6*-complemented strains relative to *sta6*.
(B) The 521 differentially expressed genes resulting directly from *STA6* were grouped according to their function in 25 categories, as assigned by MapMan ontology. For clarity, genes not assigned are not shown, but total 195.

output from this pathway resulting from increased malate synthase and isocitrate lyase activity. Increases in citrate, aconitate, and isocitrate were also noted in *sta6*. When we looked at metabolites of glycolysis and gluconeogenesis, we noted that the Fru-1,6-bisphosphate was higher in *STA6* compared with *sta6* (10.8 μM compared with 3.8 μM), consistent with increased fructose-1,6-bisphosphatase activity in the mutant. Finally, we assayed cell extract prepared at 0, 24, 48, and 96 h after N deprivation for Glc-6-P levels and determined that the level in *sta6* is unaltered at 0 and 48 h but is approximately threefold higher in *sta6* than in the complemented strain *STA6* (805 μM versus ~300 μM) at 96 h (Figure 9H). Additions of known concentrations of Glc-6-P confirmed that the assay was quantitative in this concentration range (see Supplemental Figure 7 online). These changes in metabolite levels are N-deprivation dependent, as is also the case for changes in the transcriptome (Figure 9). Therefore, we conclude that increased mRNA and protein abundance has an effect on the operation of the cognate pathways. On this basis, we suggest that the increase in Glc-6-P observed in *sta6* is a consequence of increased output from the glyoxylate and gluconeogenesis pathways, as opposed to an inability to synthesize ADP-Glc.

Acetate Assimilation Remains the Same in *sta6* and *STA6* Strains

Since genes associated with acetate assimilation are upregulated in *sta6* compared with CC-4349 and *STA6*, we wondered

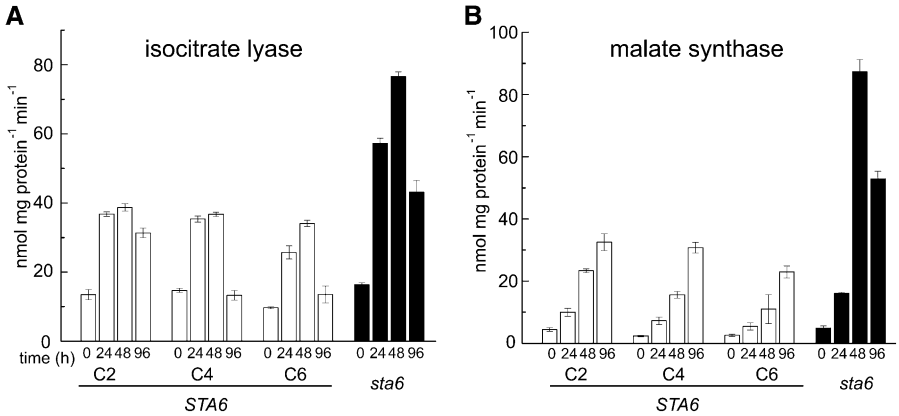

Figure 8. Increased Isocitrate Lyase and Malate Synthase Activities in *sta6* versus *STA6*.

Isocitrate lyase **(A)** and malate synthase **(B)** activities. C2, C4, and C6 represent the complemented strains (white), and *sta6* is shown in black. Extracts were prepared from cells sampled 0, 24, 48, and 96 h after removal of N. Error bars indicate the SD of three independent biological repeats.

whether the increased TAG accumulation in N-starved *sta6* cells requires greater acetate utilization from the medium. The observation that further supplementation of the medium with acetate increases TAG accumulation is consistent with this hypothesis as well (Goodson et al., 2011). Therefore, we analyzed medium from N-free cultures of all four strains at 0, 48, and 96 h after N starvation to measure acetate utilization but found that deletion of the *STA6* locus has no effect on the rate of acetate assimilation (Figure 10; see Supplemental Figure 7 online).

Genome-Wide Responses to N Deprivation

Many of the changes in the transcriptome occur in all of the strains. One documented early effect of N starvation is the

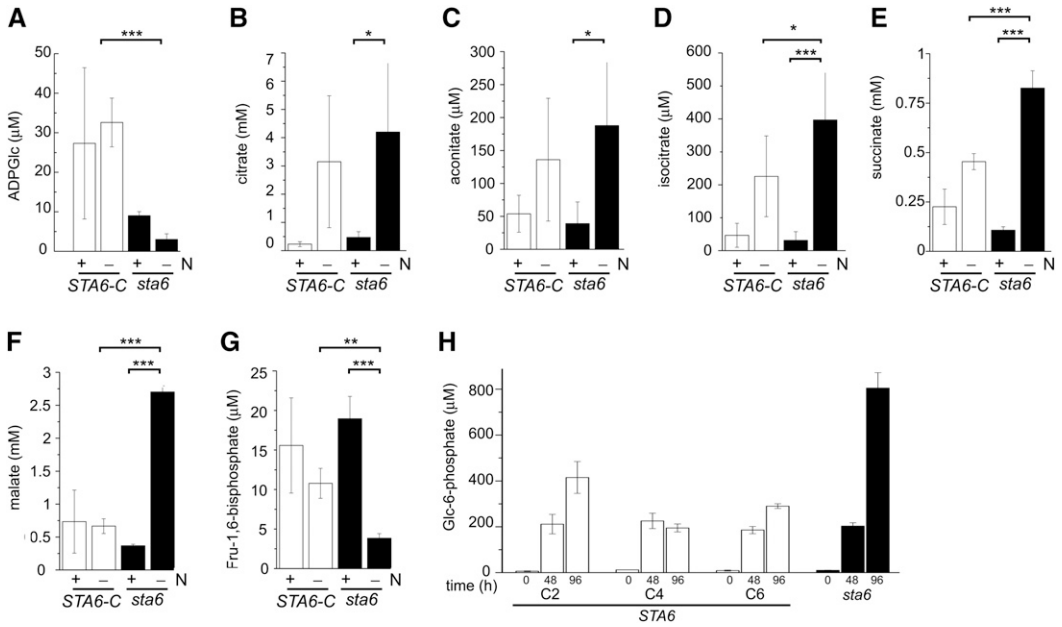

Figure 9. Metabolite Profiles in *sta6* and *STA6*-Complemented Strains Are Consistent with Predictions from Transcriptomes.

(A) to **(G)** *sta6* (black) was grown in six independent cultures, and *STA6*-C (white) comprises duplicate cultures each of *STA6*-C2, *STA6*-C4, and *STA6*-C6. Strains were cultured in +N to a density of 4×10^6 cells mL^{-1} before transferring to +N and –N cultures to a final cell density of 2×10^6 cells mL^{-1}. Samples were taken at 48 h after transfer for metabolite measurement. Significance was assessed by pairwise Student's *t* test. P value correction was performed using the Bonferroni correction method (*P < 0.05, **P < 0.01, and ***P < 0.001). Error bars represent one SD.

(H) *sta6* (black) and *STA6*-C2, *STA6*-C4, and *STA6*-C6 (white) were each grown in triplicate in +N to a density of 4×10^6 cells mL^{-1} before transferring to –N to a final cell density of 2×10^6 cells mL^{-1}. Samples were taken at 0, 48, and 96 h after transfer for Glc-6-P measurement. Error bars represent one SD.

accumulation of starch (Figure 1C). The abundances of some transcripts encoding starch biosynthesis enzymes *STA2*, *STA3* (encoding starch synthases), and *SBE1*, *SBE2*, and *SBE3* (encoding starch branching enzymes) are increased severalfold, even in *sta6* where starch is not synthesized, indicating that the increased expression of the starch synthesis pathway is a programmed response to N starvation regardless of the output from the pathway (see Supplemental Data Set 3 online). The *STA6* locus is largely deleted in the *sta6* mutant (see above and Supplemental Figure 5 online) and the reads therefore map only to the first three exons at the 5′ end. Therefore, while transcript abundance increases to 500 RPKM at 2 h (see Supplemental Data Set 3 online) for CC-4349, only a limited number of reads map to this locus in *sta6*, corresponding to ~1 RPKM. It is likely that the truncated mRNA is degraded. On the other hand, there is no difference in the pattern of expression of *STA1* (encoding the large subunit of ADP-Glc pyrophosphorylase) in *sta6* compared with CC-4349, indicating that there is no mechanism for maintaining the stoichiometry of mRNAs for the two subunits. In all strains, transcript abundances for the synthases and branching enzymes increase immediately by 0.5 h, reach a peak by 0.5 to 2 h, and are reduced to the basal level by the end of the experiment. This likely reflects the switch from starch accumulation as a short-term storage molecule to TAG for long-term storage (Siaut et al., 2011) (see Supplemental Data Set 3 online). By contrast, abundances of mRNAs encoding enzymes in lipid metabolism tend to remain relatively constant across all time points in both strains. The only transcripts whose abundances increase are those encoding some of the TAG biosynthesis-specific acyltransferases and the four glycerol-3-phosphate dehydrogenase isozymes. In particular, *GPD2* mRNA abundance increases >100-fold over the 48-h time course, from 6 to 916 RPKM and 15 to 895 in CC-4349 and *sta6*, respectively (Table 2; see Supplemental Data Set 5 online). The *DGAT1*, *DGTT1*, *DGTT2*, *DGTT3*, and *PDAT1* mRNAs encoding acyltransferases specific for TAG biosynthesis are increased approximately twofold to ~25-fold in both strains, while *DGTT4* mRNA is transiently increased shortly after N deprivation in CC-4349 (but not in *sta6*) and then remains lowly expressed throughout the experiment as in the *sta6* mutant (Table 2; see Supplemental Figure 8 online). *DGTT5* was not expressed in either strain.

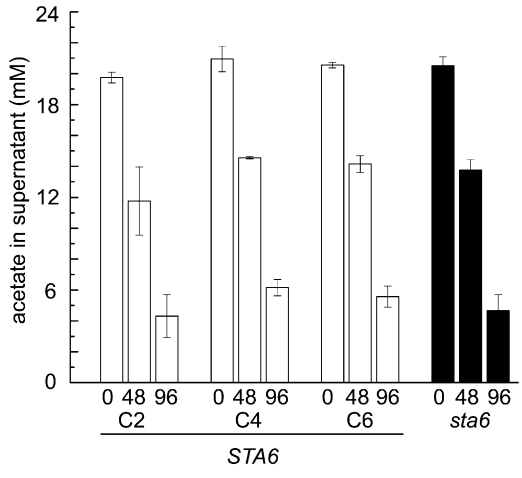

Figure 10. Acetate Utilization Is Similar in All Strains.

sta6 (black) and three independent *STA6* strains (*STA6*-C2, *STA6*-C4, and *STA6*-C6; shown in white) were cultured in +N to a density of 4×10^6 cells mL^{-1} before transferring to –N cultures to a final cell density of 2×10^6 cells mL^{-1}. Acetate levels in the supernatant were assessed at 0, 48, and 96 h after transfer to –N. Error bars represent one SD.

DISCUSSION

There are two major conclusions from this work. First, that there are substantial differences among common laboratory strains of *C. reinhardtii*, which can confound phenotypic analyses, especially when high-sensitivity assays (like RNA-Seq) are used. Therefore, it is preferable to compare mutants to complemented strains. This has its own disadvantages, including position effects that alter the expression of the complementing gene, and the possibility of deletion/rearrangement at the site of insertion of the complementing gene. However, these disadvantages can be minimized by analyzing multiple independent complementing lines. Here, we compared the *sta6* mutant to three independent complemented lines, *STA6*-C2, *STA6*-C4, and *STA6*-C6, which reduced the number of differently expressed genes to only $\sim 5 \times 10^2$. In addition, this overcomes the problem of hidden additional mutations resulting from the insertional mutagenesis protocol used for generating the mutant. In this work, we found that the *sta6* mutant is also deleted for the adjacent *RBO1* locus and indeed some of the differences between *sta6* and the purported parental *STA6* strain can perhaps be attributed to the loss of *RBO1* function. Sequence analysis of each complemented strain often readily identifies the site of insertion even with low coverage. This information can be used to assess whether the additional mutation affects the pathway of interest. Second, the comparative approach suggested increased routing of acetate toward hexose-phosphate in *sta6* compared with *STA6* under N deprivation, which we validated with measurement of enzyme activities and metabolite levels.

Mechanism of TAG Overaccumulation in *sta6*

A major objective of this study was to understand how/why *sta6* accumulates more TAG under N deprivation than does its parent. In response to N starvation stress, *C. reinhardtii* cells store carbon first as starch and then as TAG (Siaut et al., 2011). In a time-course experiment, starch accumulation was observed 1 d after N starvation but TAG accumulation did not peak until day 5. Resupply of N (coupled with a switch to darkness) resulted in rapid degradation of starch within the first few hours, whereas significant TAG degradation did not occur until more than 20 h later (Siaut et al., 2011). The pathways of carbohydrate versus lipid accumulation are thus temporally resolved. In this work, we noted that the temporal separation was not affected by the *sta6* mutation. Both strains upregulated starch synthesis genes early in response to N starvation (within 0.5 h). Transcript abundances peaked by 2 h after which they decreased rapidly (see Supplemental Data Set 3 online). Likewise, mRNAs encoding enzymes involved in starch degradation accumulated similarly in both strains,

Table 2. Abundance of mRNAs Involved in TAG Synthesis over a Time Course of 0 to 48 h

		CC-4349								*sta6*								*STA6*-C2			*STA6*-C4			*STA6*-C6		
Gene[a]	Gene Model Aug10.2	0	0.5	2	4	8	12	24	48	0	0.5	2	4	8	12	24	48	0.5	4	48	0.5	4	48	0.5	4	48
GPD1	12.g511150	5	15	11	13	15	16	19	16	8	7	6	8	10	10	9	8	8	7	14	9	6	12	7	7	14
GPD2	01.g053000	6	77	113	219	518	599	729	916	15	11	312	478	407	469	609	895	69	85	811	89	107	772	51	84	625
GPD3	01.g053150	0	0	0	1	3	5	7	8	0	0	1	2	2	2	3	5	1	1	1	0	1	1	0	0	1
GPD4	10.g421700	8	18	59	66	99	134	128	127	14	8	99	172	228	219	191	177	35	73	224	31	101	228	37	93	221
PLSB1	02.g143000	24	52	16	18	21	32	49	49	31	40	15	13	17	24	32	29	30	9	45	39	11	43	22	9	52
	06.g273250	8	21	23	16	16	22	16	15	11	12	23	18	17	20	17	16	17	15	17	17	17	14	20	16	15
KDG1	07.g312400	2	8	9	7	7	8	9	10	2	2	6	6	6	6	6	6	6	4	6	5	5	5	7	5	7
KDG2	05.g240000	37	13	17	21	20	23	17	19	38	35	13	13	18	16	14	16	13	16	12	17	14	12	14	17	13
KDG3	07.g325550	3	10	11	13	12	13	12	13	4	2	8	10	12	11	11	9	10	12	9	8	12	10	9	10	10
DGAT1	01.g045900	2	14	36	29	17	20	19	18	5	6	23	20	18	17	15	13	9	11	9	11	11	10	12	13	9
DGTT1	12.g557750	0	2	20	17	28	32	43	47	0	0	14	20	34	37	38	41	4	8	46	5	13	51	5	11	45
DGTT2	02.g121200	19	26	27	33	34	36	35	37	73	112	80	68	49	51	39	45	27	19	32	33	26	36	20	19	27
DGTT3	06.g299050	12	32	27	31	31	34	39	38	18	18	37	46	45	47	41	41	48	41	46	44	41	48	38	35	47
DGTT4	03.g205050	1	17	10	12	6	7	8	7	4	2	5	4	6	5	6	4	14	7	5	13	7	5	14	7	5
DGTT5	02.g079050	0	0	0	0	0	0	0	0	0	0	0	0	0	0	0	0	0	0	0	0	0	0	0	0	0
DGAT3-like	06.g310200	10	21	26	31	28	19	22	35	26	56	88	80	69	67	80	63	20	21	32	28	27	30	24	20	33
PDAT1	02.g106400	6	9	22	17	13	16	15	14	9	4	24	20	15	14	12	9	15	13	11	14	15	11	15	13	11
	02.g135450	10	10	10	8	6	9	12	10	11	4	7	10	10	10	11	7	13	6	7	12	6	9	12	5	9
	12.g506600	3	6	8	7	8	8	10	10	4	4	5	6	6	6	7	7	3	4	5	3	4	5	4	5	5

[a]Definitions are as follows: GPD, glycerol-3-phosphate dehydrogenase; PLSB1, glycerol-3-phosphate acyltransferase; KDG, diacylglycerol kinase; DGAT1, type 1 diacylglycerol transferase; DGTT, type-2 diacylglycerol transferase; DGAT3; type-3 diacylglycerol transferase; PDAT, phosphatidylcholine:diacylglycerol acyltransferase.

despite the absence of starch in *sta6*. Genes encoding enzymes involved in TAG synthesis showed more graduate upregulation, with mRNA abundances increasing throughout the 48-h time course (Table 2). These transcriptome level measurements are consistent with the observed rapid increase in starch accumulation compared with a later increase in TAG levels (Figures 1C and 1D).

While most of the transcriptome, including genes involved in starch and TAG metabolism, is unaffected by the function of the *STA6* gene (Figure 7), mRNAs encoding enzymes that function in acetate metabolism increased dramatically in *sta6* versus *STA6*, in particular *MAS1* and *ICL1*, which encode enzymes unique to the glyoxylate pathway. This pathway generates the 4C precursor for gluconeogenesis; indeed, *FBP1* and *PCK1*, also encoding enzymes unique to the gluconeogenesis direction, are regulated in parallel with *MAS1* and *ICL1* in N-starved *sta6* (Figure 4). Increased operation of the glyoxylate pathway and gluconeogenesis is supported by analysis of a subset of enzymes and metabolites in this work (Figures 8 and 9). Nevertheless, this result was unexpected because the movement of carbon in this direction would not be expected to stimulate fatty acid or lipid synthesis. How does this change in metabolism support increased TAG accumulation in *sta6*? Apart from the most prominent increases in *ICL1*, *MAS1*, *PCK1*, *TAL1*, and *FBP1* transcripts levels, the expression pattern of *PEPC1* and *PGM3* (and a further set of genes involved in starch synthesis like *PGI1*, *SBE2*, *SBE3*, *SSS4*, and *STA3*) is also altered in *sta6* compared with CC-4349 (Figure 3). These transcripts (like *STA6*) increase rapidly to a peak at 0.5 to 1 h and then show a partial decline in CC-4349. The initial rise is slightly delayed in *sta6*. However, it is unclear if these small differences are due to the mutation in *sta6* or to the differing genetic background, as these transcripts also showed small differences between CC-4349 and the complemented *STA6* lines.

In these experiments, *C. reinhardtii* cells were grown mixotrophically on acetate. One explanation is that *sta6* consumes more acetate than *STA6* via increased operation of acetyl-CoA synthetase and the glyoxylate pathway. Since starch synthesis is blocked, carbon is directed toward TAG. This model is consistent with the studies of others who have shown that acetate supplementation causes an increase in TAG content and the amount of acetate provided is proportional to lipid body droplet size (Goodson et al., 2011; Ramanan et al., 2013). However, when we measured acetate utilization, we found that acetate consumption was identical in both strains (Figure 10). Therefore, increased acetate utilization is not causal for increased TAG accumulation in *sta6*. It is possible that the previously reported increase in TAG resulting from provision of acetate enables cell survival and, hence, enables continuing TAG synthesis as a consequence of continued viability. Another possibility is that in the absence of ADP-Glc pyrophosphorylase activity, Glc-6-P is metabolized to trehalose, a signaling metabolite that has been identified in *C. reinhardtii* (Bölling and Fiehn, 2005). Whether trehalose levels are altered in *sta6* and, if so, whether this affects TAG synthesis remain to be tested. A third possibility is raised by the observation that *TAL1* mRNA abundance increases coordinately with that of *FBP1* and *PCK1* in N-starved *sta6* (Figure 3; see Supplemental Data Set 3 online), specifically that Glc-6-P is further metabolized by the oxidative pentose phosphate pathway. This would allow maintenance of a pool of reduced nucleotide for de novo fatty acid biosynthesis. Given that carbon availability is not the bottleneck for TAG synthesis (at least in this

genetic situation), the possibility of increased reductant availability in *sta6* being causal for TAG accumulation is intriguing. We cannot determine whether the threefold higher Glc-6-P content of *sta6* results from increased gluconeogenesis versus reduced conversion to ADP-Glc. However, the former is possibly more likely given that we observe more hexose-phosphate only in N-deprived conditions (i.e., where the glyoxylate pathway and gluconeogenesis are upregulated). If the higher Glc-6-P content of *sta6* resulted from the block in ADP-Glc synthesis, it would also be higher in N-replete conditions. On the basis of these results, we propose that future metabolic engineering projects may benefit from attempts to increase the reductant pools.

Many laboratories have monitored the expression of genes encoding TAG biosynthesis enzymes of *C. reinhardtii* under N starvation conditions (Miller et al., 2010; Boyle et al., 2012; Msanne et al., 2012; Ramanan et al., 2013). The functions of a few of these, DGTT1, PDAT1, and DGTT2, have been validated experimentally (Boyle et al., 2012; Sanjaya et al., 2013). Of seven putative acyltransferases in the *C. reinhardtii* genome, only two are differentially expressed in *sta6* versus *STA6*: *DGTT2* and Cre06.g310200, an unvalidated homolog of a type-3 acyltransferase. Acyltransferase activity has been postulated as the rate-limiting step for TAG synthesis, assuming the acyl-CoA supply is not limiting (Ichikara and Noda, 1980; Perry and Harwood, 1993; Bao and Ohlrogge, 1999). Unlike many of the mRNAs that increase in *sta6* versus *STA6*, the mRNA abundances of both *DGTT2* and Cre06.g310200 increase comparatively early (peak for DGTT2 at 0.5 h and for Cre06.g310200 at 2 h; Table 2) after initiation of the N starvation response. This indicates that these genes are upregulated independently of other genes that are differentially expressed in the two strains. Their induction might result from an unknown signaling pathway in response to a block in starch synthesis. In particular, we note that *DGTT2* is one of the 521 genes specific to the *sta6* response (Figure 5).

Finally, we observe that the increase in *MLDP1* mRNA correlates well with TAG accumulation, supporting its use as a marker for TAG content (Figure 1E), as suggested previously (Moellering and Benning, 2010). The availability of an antibody will facilitate the development of screening assays for strains with altered lipid content.

Genotype of Laboratory Strains

Several observations led to the discovery that the *cw* strain used initially in this work and prior work by others as the congenic wild-type parent of *sta6* is, in fact, unrelated. The strain has now been named CC-4349. First, the expression of mating-type specific genes in the RNA-Seq experiments indicated that CC-4349 is mt^- rather than the expected mt^+ like *sta6*. Second, the strain was larger than *sta6* and the size difference was not affected by complementation with *STA6*, suggesting other genetic differences. Most importantly, genome resequencing identified not only an order of magnitude more SNVs relative to the true parent (Table 1) but also a number of InDels. These genetic differences make it difficult to assign phenotype to the *sta6* mutation and necessitated the use of complemented strains for the comparative analyses. This is becoming more important as *C. reinhardtii* is increasingly a reference system for genetics-based studies. For the purpose of this project, we acquired the original *cw* strain (carrying the Arg auxotrophic marker) independently and found it to be the true parent by genome resequencing. There are still SNVs between this strain and the present-day *sta6*, but this is likely attributable to over a decade of laboratory propagation. The true parent is presently deposited as CC-4568. In light of these results, future work in this area should minimally compare CC-4348 and CC-4568 and ideally also CC-4565, CC-4566, and CC-4567. We also resequenced *STA6*-C6 (CC-4567) and demonstrated that this strain likely contains a single insert of the complementing genetic construct, which is at the Cre16.g66450 locus. In agreement with this, this gene, predicted to encode a calcium channel, lies within the intersect unique to *STA6*-C6 of differentially expressed genes relative to *sta6*.

In addition to deleting most of the *STA6* coding region, the neighboring gene, *RBO1*, was also partially excised in the *sta6* mutant. Insertions are often associated with deletions in the flanking DNA in *C. reinhardtii*, which may be a consequence of a missing *RAD6* (Vlcek et al., 2008). The closest homolog (mutual best hit) to *RBO1* in *Arabidopsis thaliana* is *RBOHa*, which encodes an NADPH oxidase responsible for reactive oxygen species (ROS) production in response to pathogen wounding (see Supplemental Figure 9 online). ROS signaling resulting from NADPH oxidases in vascular plants has been demonstrated in response to a number of stresses, including wounding, radiation, heat, and drought, where it induces a signaling cascade via ROS production (Torres et al., 2002). In *C. reinhardtii*, *RBO1* is induced in response to N starvation, as observed here in CC-4349 (peak of 9 RPKM in CC-4349 versus 0 in *sta6*), among other stress-inducing conditions, including Zn deprivation (Malasarn et al., 2013). Notably, two differentially expressed genes between *sta6* and CC-4349 were *LHCSR1* and *LHCSR2*, both of which are involved in photoquenching to dissipate excessive energy from high-light absorption (Peers et al., 2009; Bonente et al., 2011). Transcripts of both genes were more highly induced in CC-4349 than *sta6*. Since these stress-related mRNAs are increased in abundance in CC-4349 but not in *sta6*, we suggest that *RBO1* may have a role in the induction of these genes. In this case, the *RBO1* regulon would be expected to lie within the genes that are expressed more highly in CC-4349 versus *sta6* (see Supplemental Data Set 8 online). In this light, the deletion of the 5′ end of *RBO1*, including the first five exons, fortuitously presents the required genetic background to test this hypothesis and to define the putative *RBO1* regulon.

METHODS

Chlamydomonas reinhardtii Strains, Media, and Culture Conditions

C. reinhardtii strains used were *cw15* (*nit1 NIT2* mt^-), *sta6* (*cw15 nit1 NIT2 arg7-7 sta6*-1::*ARG7* mt^+), and three complemented strains *cw15 arg7-7 sta6-1*::*ARG7* mt^+ (*STA6*). The *cw15* and *sta6* strains are available as CC-4349 and CC-4348, respectively, from the Chlamydomonas Resource Center (CRC) (http://chlamycollection.org/; Minnesota University). The complemented *STA6* mutants, strains C2, C4, and C6, are as described previously (Li et al., 2010b) and were obtained from Ursula Goodenough (Washington University, MO). They are available as CC-4565, CC-4566, and CC-4567 from the CRC. Strain *cw15* was also obtained independently from David Dauvillée. This strain is an Arg auxotroph and

represents the true parent of *sta6*. It has been submitted to the CRC and is available as CC-4568.

Cells were grown in TAP medium unless otherwise indicated. Except where stated, cultures were grown in Innova incubators (New Brunswick Scientific) at 24°C, agitated at 180 rpm with continuous light (95 μmol m^{-2} s^{-1}, six cool white fluorescent bulbs at 4100K and three warm white fluorescent bulbs at 3000K per incubator). N minus TAP was prepared by omitting ammonium chloride, as described previously (Boyle et al., 2012), and is described as N-free media, although the amino group on Tris may be used as a N source. Briefly, cells subjected to N deprivation were grown to 4 × 10^6 mL^{-1} and collected by centrifugation at 1006*g* for 5 min at room temperature. The supernatant was discarded, and the cells were washed in N-free TAP and resuspended in the same to a final cell count of 2 × 10^6 cells mL^{-1}. Samples taken prior to washing were labeled as 0', samples taken immediately upon inoculation of N-free media were labeled as 0, and subsequent samples were labeled with respect to the time of sampling in hours. Cells were counted with a hemocytometer.

Enzyme Assays

Samples were collected at 0, 24, 48, and 96 h post N deprivation, in biological triplicate, for enzyme assays and metabolite measurements. Whole-cell lysates were prepared as follows. Eight-milliliter samples were taken at each time point, and cells were collected by centrifugation at 1006*g* for 5 min and resuspended in 1 mL of 16 mM K_2HPO_4/11 mM KH_2PO_4 buffer. Cells were broken by sonication (one 20-s pulse, amplitude 69%, using a Branson Digital Sonifier with probe model 102C), and particulate matter was removed by centrifugation at 16,100*g* for 15 min at 4°C.

Malate synthase and isocitrate lyase were assayed by modifying previously described methods (Chell and Sundaram, 1975). For malate synthase, the final reaction conditions were 30 mM imidazole, pH 8.0, 10 mM $MgCl_2$, 0.25 mM acetyl-CoA, 1 mM glyoxylic acid, 0.2 mM 5,5′-dithio-bis(2-nitrobenzoic acid), and 100 μL soluble cell extract prepared as described above per milliliter of reaction volume. Reactions were performed at 30°C and monitored at 412 nm for 5 min. For isocitrate lyase, the final reaction concentrations used were 30 mM imidazole, pH 6.8, 5 mM $MgCl_2$, 1 mM EDTA, 4 mM phenylhydrazine, and 1 mM DL-isocitric acid plus 100 μL clarified extract per milliliter of reaction. Reactions were performed at 30°C and monitored at 324 nm for 5 min. For both assays, continuous product formation was monitored for at least 5 min, and the linear portion of the product formation curve was used as a measurement of initial velocity to calculate the enzymatic activity of the clarified lysate. Reagents for all assays were from Sigma-Aldrich. All assays incorporated relevant controls to subtract background activity in which each reagent was sequentially subtracted from the reaction mixture. Assay linearity with respect to protein concentration was verified by measuring serial dilutions of the protein sample. Enzyme activities were determined relative to total protein content by the BCA assay (Thermo Scientific). Starch assays were performed using the starch assay kit (Sigma-Aldrich) according to the manufacturer's directions. Chlorophyll content of cells was measured as previously described (Moseley et al., 2002). Glc-6-P was measured using a Glc-6-P assay kit (BioVision), and concentrations were determined by comparison to a standard curve as directed by the manufacturer. The concentration of acetate in culture supernatants was determined using the EnzyChrom acetate assay kit (BioTrend Chemicals) according to the manufacturer's directions. Glc-6-P and acetate assays were performed in 96-well format and measured using a Tecan M1000 plate reader. Glc-6-P and acetate assays were validated by addition of spike-in standards (see Supplemental Figure 7 online).

Immunoblot Analysis

Soluble cell extract was prepared as described above (see Enzyme Assays). Ten micrograms of protein per sample, calculated using the BCA assay, was diluted to equal volume. Protein samples were denatured by addition of 4× Laemmli buffer (final concentration of 31.25 mM Tris, 1.525% [w/v] SDS, 5% [v/v] glycerol, 0.01% [w/v] bromophenol blue, and 5% [w/v] β-mercaptoethanol) and boiled for 10 min before separation by denaturing PAGE (12% monomer). Proteins were transferred to nitrocellulose membrane for 90 min at room temperature under constant current (1.5 mA/cm^2 membrane) in 25 mM Tris, 192 mM Gly, 0.01% (w/v) SDS, and 20% (v/v) methanol using a semidry blotter. The membranes were blocked with 1% (w/v) dried nonfat milk in phosphate buffered saline-tween (PBS-T; 137 mM NaCl, 2.7 mM KCl, 10 mM Na_2HPO_4, 1.7 mM KH_2PO_4, and 0.2% [v/v] Tween-20, adjusted to pH 7.2) for 1 h with shaking at room temperature and washed three times with 1% milk in PBS-T. Incubation of the membranes with anti-MLDP antibodies was performed at a 1:2000 dilution in 1% milk in PBS-T with shaking at room temperature for 1 h, static overnight (12 to 16 h) at 4°C, followed by shaking at room temperature for 1 h (Huang et al., 2013). After three washes with 1% milk in PBS-T and incubation with alkaline phosphatase coupled goat anti-rabbit antibody (Southern Biotechnology Associates) at a dilution of 1:2000 in 1% milk in PBS-T, antibody bound to the membrane was detected using the alkaline phosphatase color reaction. After 15 min of incubation with the color reagent, the membranes were transferred to 1× TBS, pH 7.5, and left for 14 to 16 h before imaging. ColorPlus prestained Protein Marker (Broad Range) (New England Biolabs) was used as a size standard protein.

Lipid Analysis

Lipids were analyzed by gas chromatography as described previously (Boyle et al., 2012).

Nucleic Acid Preparation and Analysis

Genomic DNA was prepared as follows. Total cellular DNA was prepared from stationary phase cultures (~1 × 10^7 cells mL^{-1}) of strains CC-4349, *sta6* (CC-4348), and *STA6-C6* (CC-4567) using standard procedures. Specifically, cells from 30 mL of each culture were collected by centrifugation (3440*g*, 5 min, 22°C) and resuspended in 2 mL of milliQ-purified water. Two milliliters of the resuspended cells was transferred to a fresh tube and combined with 2 mL of 2 × lysis solution (10 mM Tris-Cl, pH 7.5, 10 mM EDTA, 10 mM NaCl, 0.5% SDS, and 200 μg mL^{-1} proteinase K). After incubation for 2 h at 50°C, DNA was extracted by addition of 4 mL of phenol-chloroform, followed by vigorous shaking and centrifugation to separate phases (13,800*g*, 10 min, 10°C). Four milliliters of the aqueous phase was transferred to a clean tube and treated with 5 μL of 5 mg mL^{-1} of RNaseA for 30 min at 37°C, followed by an additional phenol-chloroform extraction as before. Four milliliters of the resulting aqueous phase was transferred to a clean tube. Next, polysaccharides were selectively precipitated by the addition of 1.4 mL of room temperature 100% ethanol, incubation for 15 min on wet ice, and centrifugation (13,800*g*, 10 min, 10°C). Supernatant (5.4 mL) was transferred to a clean tube, and the DNA was precipitated by the addition of 5.4 mL isopropanol, incubation for 15 min at room temperature, and centrifugation (19,800*g*, 10 min, 22°C). After he supernatant was discarded, the DNA pellets were air-dried for 15 min at room temperature, and resuspended in 525 μL of purified water. DNA was precipitated again by the addition of 100 μL of 5 M NaCl and 625 μL of 20% polyethylene glycol-8000. The mixture was incubated for 30 min on wet ice, after which the DNA was collected by centrifugation (19,800*g*, 20 min, 4°C). The supernatant was removed by decanting, and the pellet was washed with 70% ethanol, and air-dried for 15 min at room temperature. The resulting DNA was resuspended in 50 μL of purified water, and the concentration determined by optical absorbance on a NanoDrop 2000 spectrophotometer (Thermo Scientific). For each strain, 1 μg of genomic DNA was sheared by the S-220 Adaptive Focused Acoustics system

(Covaris) using the following settings: 10% duty cycle, 5.0 intensity, 200 bursts s^{-1}, 120 s, and 6°C. The resulting fragments were used to make sequencing libraries using the TruSeq DNA sample preparation kit, version 1 (Illumina), following the low-throughput protocol. The concentrations of the resulting libraries were determined by Qubit double-stranded DNA Broad Range assay kit assay kit (Invitrogen). Sequencing flow cells were prepared using the TruSeq cBot PE cluster generation kit, version 3 (Illumina), and sequencing was performed as 100 + 100-nucleotide paired end reads (CC-4349, CC-4567, CC-4568) or 50 + 50-nucleotide paired-end reads (CC-4348) on a HiSeq2000 sequencer (Illumina)

The reads were aligned using Burrows-Wheeler Aligner v.0.6.2 v.0.6.2 (Li et al., 2008), with default parameters, to the version 5.0 assembly of the *C. reinhardtii* CC-503 genome (Merchant et al., 2007). After removing duplicates with Picard MarkDuplicates (http://picard.sourceforge.net), we applied Genome Analyzer Tool Kit (McKenna et al., 2010) base quality score recalibration, InDel realignment, and small variant discovery (DePristo et al., 2011). Larger structural variants were called using BreakDancer_max1.1 (Chen et al., 2009) and Pindel0.2.4t (Ye et al., 2009), each with default parameters, followed by extensive manual filtering of false positives using IGV (Thorvaldsdóttir et al., 2012). SNVs are available at the National Center for Biotechnology Information dbSNP Short Genetic Variations database. SNVs and read alignments are available in VCF and BAM format upon request.

Samples for RNA-Seq analysis of CC-4349 and *sta6* were taken in triplicate. The RNA was prepared and assessed for integrity as previously described (Boyle et al., 2012). cDNA libraries were generated in duplicate from two of the three samples taken and sequenced on a GAIIx sequencer (Illumina) at Los Alamos National Laboratory as described (Boyle et al., 2012). The read lengths and sequence data obtained for each sample are shown in Supplemental Data Set 1 online, sheet 1. The transcriptomes of the complemented strains (CC-4565, CC-4566, and CC-4567) were determined, in comparison to *sta6* (CC-4348), in a separate experiment. In this case, only one sample was collected from each of the three independent transformants and *sta6* at each time point (see Supplemental Data Set 1 online, sheet 2), and the corresponding cDNAs sequenced on a HiSeq2000 sequencer (Illumina). Based on an estimate of library diversity and sequencing error rate, which determines the minimum score allowed in the alignment step, the sequences were mapped to the genome using alignment tools that allow for intron-like gaps (Wu and Nacu, 2010). The alignment parameters were optimized to account for the characteristic exon-intron structure of *C. reinhardtii* genes. The realignment of the existing genome annotation was used to select the class of allowed gapped alignments to the *C. reinhardtii* genome. This information was used to differentiate between unique and ambiguous alignments and to build fully mappable gene models, referred to as "mappable sets." Only unique alignments were used to compute expression estimates. Per-sample normalized coverage vectors are built from the final set of high-quality disambiguated alignments. These vectors are displayed in the form of per-base graphs on the the University of California, Santa Cruz browser hosted locally, which is available at http://genomes.mcdb.ucla.edu/. Sequence alignments and mappable sets were used to generate matrices of counts per gene. Normalization by mappable length and sequencing depth provided the matrix of expression estimates in units of RPKMs (Mortazavi et al., 2008). The counts per gene from individual experiments are analyzed for differential expression using negative binomial statistics (Anders and Huber, 2010) with predetermined levels of statistical significance (false discovery rate < 1%) and up/downregulation (a minimum of twofold) imposed to generate sets of target genes. SNVs are available at the National Center for Biotechnology Information dbSNP Short Genetic Variations database with accession numbers 902873753 - 902923703. SNVs and read alignments are available in VCF and BAM format upon request. Given the high number of regulated genes in N-free media and the size of the analyzed data sets, we classified genes according to their temporal expression profiles across individual or combined experiments. The abundances of several mRNAs were unexpectedly high at 0 and 0.5 h. We suspected this was due to the physiological stress of centrifugation and washing, as required to achieve N deprivation. To be sure there was no physiological significance, we employed qRT-PCR using cDNA from samples collected at 0' (before washing in N-free media), 0, and 0.5 h. These data reproduce the spike in transcript copy number at T0 for both *ICL1* and *FBP1* (see Supplemental Figure 10 online). Since the mRNA abundance in both strains for the two genes is >10-fold higher at T0 than in the 0' and 0.5 h samples, this suggests the increase at T0 is a response to the stress conditions the cells are exposed to. qRT-PCR was performed as previously described (Allen et al., 2007) using the primers detailed in Supplemental Table 3 online.

Genes identified by the differential expression test were clustered by a model-based clustering method implemented as previously described (Fang et al., 2012). We assumed the observed counts followed a negative binomial distribution if biological replicates were available, and a Poisson distribution otherwise. Results using 100 clusters were consolidated by visual inspection to maintain the smallest number of specific clusters as possible without losing enrichment for significant biological function (see Supplemental Figure 1 online). The clusters were complemented with functional annotations for individual or consolidated gene clusters using the pathways annotation tool (Lopez et al., 2011).

Sample Collection and Preparation for Metabolite Analyses

For metabolite analysis, cells were cultured in a shaker (180 rpm, ~75 μmol m^{-2} s^{-1} light, generated by eight cool white fluorescent bulbs). Metabolite profiles were determined according to Tohge et al. (2011). *C. reinhardtii* strains were grown in the presence or absence of N as described above in six flasks representing biological replicates. One mL of culture was added to 2 mL of 70% (v/v) methanol precooled to −70°C in an ethanol/dry ice bath in a 15-mL disposable screw-top plastic conical tube. Cells were sampled as rapidly as possible and under static light intensity (~75 μmol m^{-2} s^{-1}). After quenching, samples were immediately flash frozen in liquid N and stored at −80°C. For analysis, samples were thawed in an ethanol/dry ice bath at −35°C. Water-soluble metabolites were extracted using a slightly modified protocol as previously published (Tohge et al., 2011). Sample (525 μL) was added to 105 μL of prechilled chloroform (to −20°C) and incubated at −20°C for 1 h. The mixture was defrosted on ice, mixed vigorously for 1 min (3 × 20-s pulses and put back on ice in between), and 280 μL of ice-cold milliQ-grade water added. The mixture was agitated by vortexing, and following centrifugation at 16,100*g* in a microfuge for 5 min at 4°C, 800 μL of the upper phase was transferred to a fresh precooled 2-mL tube. Two further extractions were performed by adding 560 μL of chilled water, mixing on a vortex mixer and centrifugation to achieve a total volume of 1920 μL. This was divided into two prechilled tubes of 960 μL each. Chilled water (280 μL) was added to each aliquot, and the tubes were flash frozen and lyophilized overnight. Each sample was resuspended in 125 μL of chilled water and filtered through multiscreen filter plates Ultracel-10 (Millipore) by centrifugation for 90 min at 2300*g* at 12°C. Filtrates were analyzed by LC-MS/MS as described below.

Ion-Pair Chromatography–Triple Quadrupole Mass Spectrometry

LC-MS/MS was performed on a Dionex HPLC system coupled to a Finnigan TSQ Quantum Discovery MS-Q3 (Thermo Scientific) equipped with an electrospray ionization interface. It was operated as described (Arrivault et al., 2009) with slight modifications of the liquid chromatography gradient. Chromatographic separation was performed by passing aliquots through a Gemini (C18) 4 × 2.00-mm precolumn (Phenomenex), before separation on a Gemini (C18) 150 × 2.00-mm inner diameter, 5-μm

110 Å particle column (Phenomenex) at 35°C using a multistep gradient with online-degassed eluent A (10 mM tributylamine aqueous solution, adjusted to pH 5 with 15 mM acetic acid and 5% methanol) and eluent B (100% methanol): 0 to 5 min, 100% A; 5 to 15 min, 100 to 95% A; 15 to 22 min, 95 to 90% A; 22 to 37 min, 90 to 85% A; 37 to 40 min, 85 to 0% A, and maintained for 3 min; 43 to 47 min, 70 to 45% A, and maintained for 3 min; 50 min, 10% A, and maintained for 8 min; 58 min, 100% A, and maintained for 8 min. The flow rate was 0.2 mL·min^{-1} and was increased to 0.3 mL·min^{-1} between 22 and 58 min. After separation, compounds were ionized by electrospray ionization and detected by a triple quadrupole that was operated in negative ion mode with selected reaction monitoring using an ion spray voltage of 4000 V and a capillary temperature of 230°C. The Finnigan XCALIBUR 2.5 software (Thermo Scientific) was used for both instrument control and data acquisition. Prior to injection (100 µL), a mixture of 15 stable isotope reference compounds of known concentrations was added to the sample to correct for matrix effects on these analytes in the analysis. Metabolites were quantified by comparison of the integrated MS-Q3 signal peak area with a calibration curve obtained using authentic standards by the LCQuan software (Thermo Scientific). Further analysis was performed using Windows Excel and R statistics software (R version 2.9.2 and 2.14.1 provided by the Comprehensive R Archive Network (CRAN) project, http://www.R-project.org).

Accession Numbers

Sequence data from this article can be found in the GenBank/EMBL databases under the accession number GSE51642, and the dbSNP Short Genetic Variations database with accession numbers 902873753 - 902923703.

Supplemental Data

The following materials are available in the online version of this article.

Supplemental Figure 1. Differential Responses of CC-4349 and *sta6* to N Starvation.

Supplemental Figure 2. Greater Upregulation of Genes Encoding Enzymes of Acetate Metabolism, Gluconeogenesis, and the Oxidative Pentose Phosphate Pathway in *sta6* versus *STA6*.

Supplemental Figure 3. Mating-Type Genes Used to Distinguish Relationship of Strains.

Supplemental Figure 4. Size Phenotype of *sta6* Is Not Rescued by the *STA6* Gene.

Supplemental Figure 5. Coverage Graph Identifies the Lesion at the *STA6* Locus.

Supplemental Figure 6. Evolutionary Relationships of Strains.

Supplemental Figure 7. Spike-in Controls Indicate Enzyme-Based Assays Are Quantitative.

Supplemental Figure 8. Expression Profiles of Genes Related to TAG Accumulation.

Supplemental Figure 9. Similarity between *RBO1*, *RBO2*, and *RBOHA*.

Supplemental Figure 10. qRT-PCR Suggests the Increase in mRNA Abundance Observed at T0 Is a Consequence of Centrifugation and Cell Resuspension Stress.

Supplemental Figure 11. Oxidative Pentose Phosphate Pathway.

Supplemental Table 1. Genome Sequence Libraries.

Supplemental Table 2. Mutations of *sta6*, CC-4349, and *STA6*-C6 Compared with the Reference Strain CC-503.

Supplemental Table 3. Primer Sequences Used for qRT-PCR.

Supplemental Data Set 1. RNA-Seq Libraries.

Supplemental Data Set 2. Transcripts with Increased Abundance in sta6 versus CC-4349.

Supplemental Data Set 3. Abundance of mRNAs Involved in Central Carbon Metabolism.

Supplemental Data Set 4. Comparison of mRNA Abundances for Genes Encoding Enzymes Relating to Photosynthesis and Chlorophyll Synthesis and Degradation.

Supplemental Data Set 5. Comparison of mRNA Abundances for Genes Encoding Enzymes Relating to Lipid Metabolism.

Supplemental Data Set 6. Comparison of mRNA Abundances for Genes Encoding Enzymes Relating to Gametogenesis.

Supplemental Data Set 7. *STA6*-Responsive Genes.

Supplemental Data Set 8. RNAs with Increased Abundance in CC-4349 versus *sta6.*

ACKNOWLEDGMENTS

This work was supported by Department of Energy Contract DE-EE0003046 (to S.S.M., M.P., and S.J. via the National Alliance for Advance Biofuels and Bioproducts Consortium) and in part by the National Institutes of Health R24 GM092473 to S.S.M. and the U.S. Air Force Office of Scientific Research (FA9550-11-10264, to C.B.). I.K.B. is supported by a training grant from the National Institutes of Health (T32 ES015457). We thank Ursula Goodenough for forwarding us strains *cw15* (CC-4349), *sta6* (CC-4348), *STA6*-C2 (CC-4565), *STA6*-C4 (CC-4566), and *STA6*-C6 (CC-4567), David Dauvillée for an independent *cw15* (CC-4568), and Anthony Huang for the MLDP1 antibody.

AUTHOR CONTRIBUTIONS

S.S.M., I.K.B., N.R.B., and D.C. designed the experiments. I.K.B., A.G.G., S.F.-G., T.M., S.D.G., B.L., N.R.B., and J.K. performed the experiments. D.C. performed the bioinformatic analysis of RNA-Seq data. S.J. generated libraries for RNA-Seq and supervised sequencing the transcriptomes. M.P. supervised all bioinformatic analysis. C.B. supervised lipid analysis. M.S. supervised the metabolite analysis. I.K.B., S.S.M., and S.F.-G. analyzed the data. S.S.M. and I.K.B. prepared and edited the article. All authors commented on and revised the article.

Received August 17, 2013; revised October 8, 2013; accepted October 31, 2013; published November 26, 2013.

REFERENCES

Allen, M.D., del Campo, J.A., Kropat, J., and Merchant, S.S. (2007). *FEA1*, *FEA2*, and *FRE1*, encoding two homologous secreted proteins and a candidate ferrireductase, are expressed coordinately with *FOX1* and *FTR1* in iron-deficient *Chlamydomonas reinhardtii*. Eukaryot. Cell **6:** 1841–1852.

Anders, S., and Huber, W. (2010). Differential expression analysis for sequence count data. Genome Biol. **11:** R106.

Arrivault, S., Guenther, M., Ivakov, A., Feil, R., Vosloh, D., van Dongen, J.T., Sulpice, R., and Stitt, M. (2009). Use of reverse-phase liquid chromatography, linked to tandem mass spectrometry, to profile the Calvin cycle and other metabolic intermediates in Arabidopsis rosettes at different carbon dioxide concentrations. Plant J. **59:** 826–839.

Atteia, A., et al. (2009). A proteomic survey of *Chlamydomonas reinhardtii* mitochondria sheds new light on the metabolic plasticity of the organelle and on the nature of the alpha-proteobacterial mitochondrial ancestor. Mol. Biol. Evol. **26:** 1533–1548.

Ball, S., and Deschamps, P. (2009). Starch metabolism. In The Chlamydomonas Sourcebook, Vol. 2. (San Diego, CA: Academic Press).

Ball, S., Marianne, T., Dirick, L., Fresnoy, M., Delrue, B., and Decq, A. (1991). A *Chlamydomonas reinhardtii* low-starch mutant is defective for 3-phosphoglycerate activation and orthophosphate inhibition of ADP-glucose pyrophosphorylase. Planta **185:** 17–26.

Bao, X., and Ohlrogge, J. (1999). Supply of fatty acid is one limiting factor in the accumulation of triacylglycerol in developing embryos. Plant Physiol. **120:** 1057–1062.

Beck, C., and Haring, M. (1996). Gametic differentiation of Chlamydomonas. Int. Rev. Cytol. **168:** 259–302.

Boyle, N.R., et al. (2012). Three acyltransferases and nitrogen-responsive regulator are implicated in nitrogen starvation-induced triacylglycerol accumulation in Chlamydomonas. J. Biol. Chem. **287:** 15811–15825.

Breuer, G., Lamers, P.P., Martens, D.E., Draaisma, R.B., and Wijffels, R.H. (2012). The impact of nitrogen starvation on the dynamics of triacylglycerol accumulation in nine microalgae strains. Bioresour. Technol. **124:** 217–226.

Brueggeman, A.J., Gangadharaiah, D.S., Cserhati, M.F., Casero, D., Weeks, D.P., and Ladunga, I. (2012). Activation of the carbon concentrating mechanism by CO_2 deprivation coincides with massive transcriptional restructuring in *Chlamydomonas reinhardtii*. Plant Cell **24:** 1860–1875.

Bulté, L., and Wollman, F.A. (1992). Evidence for a selective destabilization of an integral membrane protein, the cytochrome b_6/*f* complex, during gametogenesis in *Chlamydomonas reinhardtii*. Eur. J. Biochem. **204:** 327–336.

Bölling, C., and Fiehn, O. (2005). Metabolite profiling of *Chlamydomonas reinhardtii* under nutrient deprivation. Plant Physiol. **139:** 1995–2005.

Bonente, G., Ballottari, M., Truong, T.B., Morosinotto, T., Ahn, T.K., Fleming, G.R., Niyogi, K.K., and Bassi, R. (2011). Analysis of LhcSR3, a protein essential for feedback de-excitation in the green alga *Chlamydomonas reinhardtii*. PLoS Biology **9:** e1000577–e1000577.

Cakmak, T., Angun, P., Demiray, Y.E., Ozkan, A.D., Elibol, Z., and Tekinay, T. (2012). Differential effects of nitrogen and sulfur deprivation on growth and biodiesel feedstock production of *Chlamydomonas reinhardtii*. Biotechnol. Bioeng. **109:** 1947–1957.

Catalanotti, C., Dubini, A., Subramanian, V., Yang, W., Magneschi, L., Mus, F., Seibert, M., Posewitz, M.C., and Grossman, A.R. (2012). Altered fermentative metabolism in *Chlamydomonas reinhardtii* mutants lacking pyruvate formate lyase and both pyruvate formate lyase and alcohol dehydrogenase. Plant Cell **24:** 692–707.

Chell, R.M., and Sundaram, T.K. (1975). Isolation and characterization of isocitrate lyase and malate synthase from *Bacillus stearothermophilus*. Biochem. Soc. Trans. **3:** 303–306.

Chen, K., et al. (2009). BreakDancer: An algorithm for high-resolution mapping of genomic structural variation. Nat. Methods **6:** 677–681.

DePristo, M.A., et al. (2011). A framework for variation discovery and genotyping using next-generation DNA sequencing data. Nat. Genet. **43:** 491–498.

Fan, J., Andre, C., and Xu, C. (2011). A chloroplast pathway for the de novo biosynthesis of triacylglycerol in *Chlamydomonas reinhardtii*. FEBS Lett. **585:** 1985–1991.

Fan, J., Yan, C., Andre, C., Shanklin, J., Schwender, J., and Xu, C. (2012). Oil accumulation is controlled by carbon precursor supply for fatty acid synthesis in *Chlamydomonas reinhardtii*. Plant Cell Physiol. **53:** 1380–1390.

Fang, W., Si, Y., Douglass, S., Casero, D., Merchant, S.S., Pellegrini, M., Ladunga, I., Liu, P., and Spalding, M.H. (2012). Transcriptome-wide changes in *Chlamydomonas reinhardtii* gene expression regulated by carbon dioxide and the CO_2-concentrating mechanism regulator *CIA5/CCM1*. Plant Cell **24:** 1876–1893.

Ferris, P.J., Armbrust, E.V., and Goodenough, U.W. (2002). Genetic structure of the mating-type locus of *Chlamydomonas reinhardtii*. Genetics **160:** 181–200.

Ferris, P.J., and Goodenough, U.W. (1994). The mating-type locus of *Chlamydomonas reinhardtii* contains highly rearranged DNA sequences. Cell **76:** 1135–1145.

Ferris, P.J., Woessner, J.P., and Goodenough, U.W. (1996). A sex recognition glycoprotein is encoded by the plus mating-type gene *fus1* of *Chlamydomonas reinhardtii*. Mol. Biol. Cell **7:** 1235–1248.

Goodson, C., Roth, R., Wang, Z.T., and Goodenough, U. (2011). Structural correlates of cytoplasmic and chloroplast lipid body synthesis in *Chlamydomonas reinhardtii* and stimulation of lipid body production with acetate boost. Eukaryot. Cell **10:** 1592–1606.

Granum, E., Kirkvold, S., and Myklestad, S. (2002). Cellular and extracellular production of carbohydrates and amino acids by the marine diatom *Skeletonema costatum*: Diel variations and effects of N depletion. Mar. Ecol. Prog. Ser. **242:** 83–94.

Guschina, I.A., and Harwood, J.L. (2006). Lipids and lipid metabolism in eukaryotic algae. Prog. Lipid Res. **45:** 160–186.

Harris, E.H. (2001). Chlamydomonas as a model organism. Annu. Rev. Plant Physiol. Plant Mol. Biol. **52:** 363–406.

Hernández, M.L., Whitehead, L., He, Z., Gazda, V., Gilday, A., Kozhevnikova, E., Vaistij, F.E., Larson, T.R., and Graham, I.A. (2012). A cytosolic acyltransferase contributes to triacylglycerol synthesis in sucrose-rescued Arabidopsis seed oil catabolism mutants. Plant Physiol. **160:** 215–225.

Hu, Q., Sommerfeld, M., Jarvis, E., Ghirardi, M., Posewitz, M., Seibert, M., and Darzins, A. (2008). Microalgal triacylglycerols as feedstocks for biofuel production: Perspectives and advances. Plant J. **54:** 621–639.

Huang, N.L., Huang, M.D., Chen, T.L., and Huang, A.H. (2013). Oleosin of subcellular lipid droplets evolved in green algae. Plant Physiol. **161:** 1862–1874.

Ichikara, K.I., and Noda, M. (1980). Fatty acid composition and lipid synthesis in developing safflower seed. Phytochemistry **19:** 49–54.

Johnson, X., and Alric, J. (2012). Interaction between starch breakdown, acetate assimilation, and photosynthetic cyclic electron flow in *Chlamydomonas reinhardtii*. J. Biol. Chem. **287:** 26445–26452.

Johnson, X., and Alric, J. (2013). Central carbon metabolism and electron transport in *Chlamydomonas reinhardtii*: Metabolic constraints for carbon partitioning between oil and starch. Eukaryot. Cell **12:** 776–793.

Kropat, J., Hong-Hermesdorf, A., Casero, D., Ent, P., Castruita, M., Pellegrini, M., Merchant, S.S., and Malasarn, D. (2011). A revised mineral nutrient supplement increases biomass and growth rate in *Chlamydomonas reinhardtii*. Plant J. **66:** 770–780.

Lardizabal, K.D., Mai, J.T., Wagner, N.W., Wyrick, A., Voelker, T., and Hawkins, D.J. (2001). DGAT2 is a new diacylglycerol acyltransferase gene family: Purification, cloning, and expression in insect cells of two polypeptides from *Mortierella ramanniana* with diacylglycerol acyltransferase activity. J. Biol. Chem. **276:** 38862–38869.

Li, Y., Han, D., Hu, G., Dauvillee, D., Sommerfeld, M., Ball, S., and Hu, Q. (2010b). Chlamydomonas starchless mutant defective in ADP-glucose pyrophosphorylase hyper-accumulates triacylglycerol. Metab. Eng. **12:** 387–391.

Li, Y., Han, D., Hu, G., Sommerfeld, M., and Hu, Q. (2010a). Inhibition of starch synthesis results in overproduction of lipids in *Chlamydomonas reinhardtii*. Biotechnol. Bioeng. **107:** 258–268.

Li, H., Ruan, J., and Durbin, R.D.A.N. (2008). Mapping short DNA sequencing reads and calling variants using mapping quality scores. Genome Res **18:** 1851–1858.

Li-Beisson, Y., et al. (2010). Acyl-lipid metabolism. The Arabidopsis Book, **8:** e0133 doi: 10.1199/tab.0133.

Lin, H., and Goodenough, U.W. (2007). Gametogenesis in the *Chlamydomonas reinhardtii* minus mating type is controlled by two genes, *MID* and *MTD1.* Genetics **176:** 913–925.

Lopez, D., Casero, D., Cokus, S.J., Merchant, S.S., and Pellegrini, M. (2011). Algal Functional Annotation Tool: A web-based analysis suite to functionally interpret large gene lists using integrated annotation and expression data. BMC Bioinformatics **12:** 282

Malasarn, D., Kropat, J., Hsieh, S.I., Finazzi, G., Casero, D., Loo, J.A., Pellegrini, M., Wollman, F.-A., and Merchant, S.S. (2013). Zinc deficiency impacts CO_2 assimilation and disrupts copper homeostasis in *Chlamydomonas reinhardtii*. J. Biol. Chem. **288:** 10672–10683.

Martin, N.C., and Goodenough, U.W. (1975). Gametic differentiation in *Chlamydomonas reinhardtii.* I. Production of gametes and their fine structure. J. Cell Biol. **67:** 587–605.

Matthew, T., Zhou, W., Rupprecht, J., Lim, L., Thomas-Hall, S.R., Doebbe, A., Kruse, O., Hankamer, B., Marx, U.C., Smith, S.M., and Schenk, P.M. (2009). The metabolome of *Chlamydomonas reinhardtii* following induction of anaerobic H_2 production by sulfur depletion. J. Biol. Chem. **284:** 23415–23425.

May, P., Wienkoop, S., Kempa, S., Usadel, B., Christian, N., Rupprecht, J., Weiss, J., Recuenco-Munoz, L., Ebenhöh, O., Weckwerth, W., and Walther, D. (2008). Metabolomics- and proteomics-assisted genome annotation and analysis of the draft metabolic network of *Chlamydomonas reinhardtii*. Genetics **179:** 157–166.

McKenna, A., Hanna, M., Banks, E., Sivachenko, A., Cibulskis, K., Kernytsky, A., Garimella, K., Altshuler, D., Gabriel, S., Daly, M., and DePristo, M.A. (2010). The Genome Analysis Toolkit: A MapReduce framework for analyzing next-generation DNA sequencing data. Genome Res. **20:** 1297–1303.

Merchant, S.S., Kropat, J., Liu, B., Shaw, J., and Warakanont, J. (2012). TAG, you're it! Chlamydomonas as a reference organism for understanding algal triacylglycerol accumulation. Curr. Opin. Biotechnol. **23:** 352–363.

Merchant, S.S., et al. (2007). The Chlamydomonas genome reveals the evolution of key animal and plant functions. Science **318:** 245–250.

Miller, R., et al. (2010). Changes in transcript abundance in *Chlamydomonas reinhardtii* following nitrogen deprivation predict diversion of metabolism. Plant Physiol. **154:** 1737–1752.

Moellering, E.R., and Benning, C. (2010). RNA interference silencing of a major lipid droplet protein affects lipid droplet size in *Chlamydomonas reinhardtii*. Eukaryot. Cell **9:** 97–106.

Mortazavi, A., Williams, B.A., McCue, K., Schaeffer, L., and Wold, B. (2008). Mapping and quantifying mammalian transcriptomes by RNA-Seq. Nat. Methods **5:** 621–628.

Moseley, J.L., Page, M.D., Alder, N.P., Eriksson, M., Quinn, J., Soto, F., Theg, S.M., Hippler, M., and Merchant, S. (2002). Reciprocal expression of two candidate di-iron enzymes affecting photosystem I and light-harvesting complex accumulation. Plant Cell **14:** 673–688.

Mouille, G., Maddelein, M.L., Libessart, N., Talaga, P., Decq, A., Delrue, B., and Ball, S. (1996). Preamylopectin processing: A mandatory step for starch biosynthesis in plants. Plant Cell **8:** 1353–1366.

Msanne, J., Xu, D., Konda, A.R., Casas-Mollano, J.A., Awada, T., Cahoon, E.B., and Cerutti, H. (2012). Metabolic and gene expression changes triggered by nitrogen deprivation in the photoautotrophically grown microalgae *Chlamydomonas reinhardtii* and *Coccomyxa* sp. C-169. Phytochemistry **75:** 50–59.

Mühlhaus, T., Weiss, J., Hemme, D., Sommer, F., and Schroda, M. (2011). Quantitative shotgun proteomics using a uniform ^{15}N-labeled standard to monitor proteome dynamics in time course experiments reveals new insights into the heat stress response of *Chlamydomonas reinhardtii*. Mol. Cell. Proteomics **10:** 004739.

Pan, J., and Snell, W.J. (2000). Signal transduction during fertilization in the unicellular green alga, Chlamydomonas. Curr. Opin. Microbiol. **3:** 596–602.

Pavlidis, P., and Noble, W.S. (2003). Matrix2png: A utility for visualizing matrix data. Bioinformatics **19:** 295–296.

Peers, G., Truong, T.B., Ostendorf, E., Busch, A., Elrad, D., Grossman, A.R., Hippler, M., and Niyogi, K.K. (2009). An ancient light-harvesting protein is critical for the regulation of algal photosynthesis. Nature **462:** 518–521.

Perry, H.J., and Harwood, J.L. (1993). Radiolabelling studies of acyl lipids in developing seeds of *Brassica napus*: Use of [1-^{14}C]acetate precursor. Phytochemistry **33:** 329–333.

Plumley, F.G., and Schmidt, G.W. (1989). Nitrogen-dependent regulation of photosynthetic gene expression. Proc. Natl. Acad. Sci. USA **86:** 2678–2682.

Ramanan, R., Kim, B.H., Cho, D.H., Ko, S.R., Oh, H.M., and Kim, H. S. (2013). Lipid droplet synthesis is limited by acetate availability in starchless mutant of *Chlamydomonas reinhardtii*. FEBS Lett. **587:** 370–377.

Ramazanov, A., and Ramazanov, Z. (2006). Isolation and characterization of a starchless mutant of *Chlorella pyrenoidosa* STL-PI with a high growth rate, and high protein and polyunsaturated fatty acid content. Phycol. Res. **54:** 255–259.

Rani, S.H., Krishna, T.H.A., Saha, S., Negi, A.S., and Rajasekharan, R. (2010). Defective in cuticular ridges (DCR) of *Arabidopsis thaliana*, a gene associated with surface cutin formation, encodes a soluble diacylglycerol acyltransferase. J. Biol. Chem. **285:** 38337–38347.

Rodolfi, L., Chini Zittelli, G., Bassi, N., Padovani, G., Biondi, N., Bonini, G., and Tredici, M.R. (2009). Microalgae for oil: Strain selection, induction of lipid synthesis and outdoor mass cultivation in a low-cost photobioreactor. Biotechnol. Bioeng. **102:** 100–112.

Rolland, N., Atteia, A., Decottignies, P., Garin, J., Hippler, M., Kreimer, G., Lemaire, S.D., Mittag, M., and Wagner, V. (2009). Chlamydomonas proteomics. Curr. Opin. Microbiol. **12:** 285–291.

Sager, R., and Granick, S. (1954). Nutritional control of sexuality in *Chlamydomonas reinhardi*. J. Gen. Physiol. **37:** 729–742.

Saha, S., Enugutti, B., Rajakumari, S., and Rajasekharan, R. (2006). Cytosolic triacylglycerol biosynthetic pathway in oilseeds. Molecular cloning and expression of peanut cytosolic diacylglycerol acyltransferase. Plant Physiol. **141:** 1533–1543.

Sanjaya, D., Durrett, T.P., Weise, S.E., and Benning, C. (2011). Increasing the energy density of vegetative tissues by diverting carbon from starch to oil biosynthesis in transgenic *Arabidopsis*. Plant Biotechnol. J. **9:** 874–883.

Sanjaya, M., Miller, R., Durrett, T.P., Kosma, D.K., Lydic, T.A., Muthan, B., Koo, A.J., Bukhman, Y.V., Reid, G.E., Howe, G.A., Ohlrogge, J., and Benning, C. (2013). Altered lipid composition and enhanced nutritional value of *Arabidopsis* leaves following introduction of an algal diacylglycerol acyltransferase 2. Plant Cell **25:** 677–693.

Siaut, M., Cuiné, S., Cagnon, C., Fessler, B., Nguyen, M., Carrier, P., Beyly, A., Beisson, F., Triantaphylidès, C., Li-Beisson, Y., and Peltier, G. (2011). Oil accumulation in the model green alga *Chlamydomonas reinhardtii*: Characterization, variability between common laboratory strains and relationship with starch reserves. BMC Biotechnol. **11:** 7.

Siersma, P.W., and Chiang, K.S. (1971). Conservation and degradation of cytoplasmic and chloroplast ribosomes in *Chlamydomonas reinhardtii*. J. Mol. Biol. **58:** 167–185.

Smith, A.M. (1999). Making starch. Curr. Opin. Plant Biol. **2:** 223–229.

Torres, M.A., Dangl, J.L., and Jones, J.D.G. (2002). Arabidopsis gp91phox homologues AtrbohD and AtrbohF are required for accumulation of reactive oxygen intermediates in the plant defense response. Proc. Natl. Acad. Sci. USA **99:** 517–522.

Urzica, E.I., Casero, D., Yamasaki, H., Hsieh, S.I., Adler, L.N., Karpowicz, S.J., Blaby-Haas, C.E., Clarke, S.G., Loo, J.A., Pellegrini, M., and Merchant, S.S. (2012). Systems and trans-system level analysis identifies conserved iron deficiency responses in the plant lineage. Plant Cell **24:** 3921–3948.

Varum, K.M., and Myklestad, S. (1984). Effects of light, salinity and nutrient limitation on the production of β-1,3-D-glucan and exo-d-glucanase activity in *Skeletonema costatum* (grev.) cleve. J. Exp. Mar. Biol. Ecol. **83:** 13–25.

Vlcek, D., Sevcovicová, A., Sviezená, B., Gálová, E., and Miadoková, E. (2008). *Chlamydomonas reinhardtii:* A convenient model system for the study of DNA repair in photoautotrophic eukaryotes. Curr. Genet. **53:** 1–22.

Wang, H., Alvarez, S., and Hicks, L.M. (2012). Comprehensive comparison of iTRAQ and label-free LC-based quantitative proteomics approaches using two *Chlamydomonas reinhardtii* strains of interest for biofuels engineering. J. Proteome Res. **11:** 487–501.

Wang, Z.T., Ullrich, N., Joo, S., Waffenschmidt, S., and Goodenough, U. (2009). Algal lipid bodies: Stress induction, purification, and biochemical characterization in wild-type and starchless *Chlamydomonas reinhardtii*. Eukaryot. Cell **8:** 1856–1868.

Wattebled, F., Buléon, A., Bouchet, B., Ral, J.-P., Liénard, L., Delvallé, D., Binderup, K., Dauvillée, D., Ball, S., and D'Hulst, C. (2002). Granule-bound starch synthase I. A major enzyme involved in the biogenesis of B-crystallites in starch granules. Eur. J. Biochem. **269:** 3810–3820.

Wattebled, F., Ral, J.P., Dauvillée, D., Myers, A.M., James, M.G., Schlichting, R., Giersch, C., Ball, S.G., and D'Hulst, C. (2003). *STA11*, a *Chlamydomonas reinhardtii* locus required for normal starch granule biogenesis, encodes disproportionating enzyme. Further evidence for a function of α-1,4 glucanotransferases during starch granule biosynthesis in green algae. Plant Physiol. **132:** 137–145.

Work, V.H., Radakovits, R., Jinkerson, R.E., Meuser, J.E., Elliott, L.G., Vinyard, D.J., Laurens, L.M.L., Dismukes, G.C., and Posewitz, M.C. (2010). Increased lipid accumulation in the *Chlamydomonas reinhardtii sta7-10* starchless isoamylase mutant and increased carbohydrate synthesis in complemented strains. Eukaryot. Cell **9:** 1251–1261.

Wu, T.D., and Nacu, S. (2010). Fast and SNP-tolerant detection of complex variants and splicing in short reads. Bioinformatics **26:** 873–881.

Ye, K., Schulz, M.H., Long, Q., Apweiler, R., and Ning, Z. (2009). Pindel: A pattern growth approach to detect break points of large deletions and medium sized insertions from paired-end short reads. Bioinformatics **25:** 2865–2871.

Yoon, K., Han, D., Li, Y., Sommerfeld, M., and Hu, Q. (2012). Phospholipid:diacylglycerol acyltransferase is a multifunctional enzyme involved in membrane lipid turnover and degradation while synthesizing triacylglycerol in the unicellular green microalga *Chlamydomonas reinhardtii*. Plant Cell **24:** 3708–3724.

Zabawinski, C., Van Den Koornhuyse, N., D'Hulst, C., Schlichting, R., Giersch, C., Delrue, B., Lacroix, J.-M., Preiss, J., and Ball, S. (2001). Starchless mutants of *Chlamydomonas reinhardtii* lack the small subunit of a heterotetrameric ADP-glucose pyrophosphorylase. J. Bacteriol. **183:** 1069–1077.

Zeeman, S.C., Kossmann, J., and Smith, A.M. (2010). Starch: Its metabolism, evolution, and biotechnological modification in plants. Annu. Rev. Plant Biol. **61:** 209–234.